EUROPEAN ORGANIZATION FOR NUCLEAR RESEARCH

CERN-EP/84-168
17 December 1984

THE EXPERIMENTAL METHOD OF RING-IMAGING CHERENKOV (RICH) COUNTERS

T. Ekelöf*)
University of Uppsala, Sweden

ABSTRACT

The resolution, the optics design criteria and the expected particle-discrimination performance of RICH counters for use in particle collider experiments are discussed.

Lectures given at the
1984 SLAC Summer Institute on Particle Physics,
Stanford Linear Accelerator Center,
Stanford, California, USA,
23 July–3 August 1984.

---

*) Presently visitor at CERN, Geneva, Switzerland.

1. INTRODUCTION

This year we celebrate the 50th anniversary of the discovery of Cherenkov radiation by P.A. Cherenkov [1] in Moscow. This kind of radiation is basically a electromagnetic shock-wave phenomenon, analagous in form to the more familiar shock-wave phenomena in classical physics of front-wave emission from a boat in water and acoustic bang-wave emission from a supersonic aeroplane. In all three cases the shock wave can be described as the result of constructive interference of spherical (circular) waves emitted by an object (the emitter e) travelling in a medium (m) along a straight path with a speed v_e that exceeds the wave-propagation velocity (group velocity) v_m in the medium. The angle of emission θ of the shock wave with regard to the trajectory of the object is straightforwardly obtained using Huygens' principle as illustrated in Fig. 1;

$$\theta = \arccos (v_m/v_e) . \tag{1}$$

For a charged particle travelling in a transparent dielectric medium of refractive index n we may express the two velocities as

$$v_e = \beta c \tag{2}$$

$$v_m = c/n, \tag{3}$$

which inserted in Eq. (1) yields

$$\theta = \arccos (1/\beta n) . \tag{4}$$

This relation can also be derived from classical electrodynamics considering the angular distribution of energy radiated from a current density (defined in this case by the moving charged particle) in a homogeneous dielectric [2]. The radiation distribution is found to have a sharp maximum at the polar angle $\arccos(1/\beta n)$. The classical relation (1) can thus be used also for relativistic velocities. Note, however, that since in the classical case v_e can be much larger than v_m, θ may approach 90° when v_e is very large. Since in the relativistic case β cannot be larger than unity θ will not exceed the angle $\arccos (1/n)$. The Cherenkov angle thus grows from $\theta = 0$ at the threshold velocity $\beta = 1/n$ up to a maximum value $\theta = \arccos (1/n)$ as β approaches unity. In Table 1 the refractive index for visible light and the maximum Cherenkov angle are given for some familiar gases, liquids, and solids.

When dealing with relativistic elementary particles it is often more convenient to use the Lorenz variable

$$\gamma = E/m = 1/\sqrt{1 - \beta^2} \tag{5}$$

to specify the velocity of the particle rather than the relative velocity β ($= v/c = p/E = \sqrt{1 - 1/\gamma^2}$). This is so because for a given particle of mass m at highly relativistic energy,

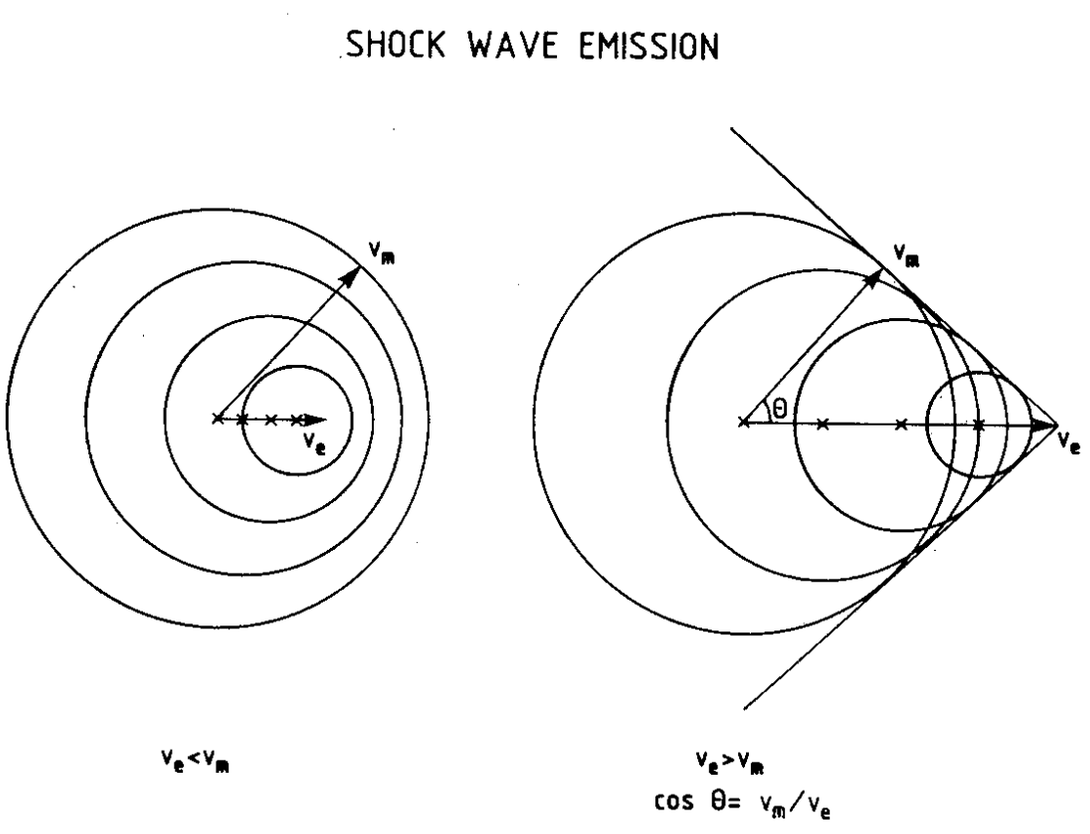

Fig. 1 Shock-wave formation by an object e that travels through a medium m emitting spherical waves. If $v_e > v_m$ a shock-wave is formed according to Huygens' principle (right). If $v_e < v_m$ no shock wave is formed (left).

γ is approximately proportional to the momentum p ($\gamma = E/m = \sqrt{p^2 + m^2}/m \approx p/m$ for $p \gg m$). The momentum can be determined from the curvature of the charged-particle track in a magnetic field. Measuring both p and γ, an approximate value of the mass of the particle is thus simply obtained as the ratio between the two.

Table 1

Refractive index for visible light, maximal Cherenkov angle and number of Cherenkov photons emitted from a 10 cm long track in a few well-known gases, liquids, and solids.

	n	θ_{max} (°)	$N_{ph\ vis}$ (10 cm)
Helium	1.000035	0.48	0.39
Air	1.000283	1.36	3.14
Isobutane	1.00127	2.89	14.07
Freon	1.233	35.8	1899
Water	1.33	41.2	2412
Quartz	1.46	46.7	2946
BGO	2.15	62.3	4349

Expressed in γ the previously discussed results take the form

$$\theta = \arccos\left[1/(n \cdot \sqrt{1 - 1/\gamma^2})\right] \tag{6}$$

For $\gamma \to \infty$:

$$\theta_{max} = \arccos(1/n) \tag{7}$$

For $\theta \to 0$:

$$\gamma_{threshold} = 1/\sqrt{1 - 1/n^2} \tag{8}$$

According to classical electrodynamics, the power radiated in a given direction by an electric current depends only on the component of the current that is perpendicular to the direction of the observed radiation. Hence, if Cherenkov radiation occurs at a certain angle θ with regard to the direction of the charged-particle motion, then the component of the current that contributes to the radiation is proportional to $\sin\theta$. As the power is proportional to the square of the current the intensity of the Cherenkov light is proportional to $\sin^2\theta$. The full electrodynamical expression for the number of emitted Cherenkov photons is [2]

$$N_\gamma = (e^2/\hbar c^2) \cdot L \cdot \sin^2\theta \cdot \Delta\omega\,, \tag{9}$$

where L is the length of the particle track in the dielectric and $\Delta\omega$ is the width of the frequency band over which photons are detected. This relation also expresses the important fact that Cherenkov radiation is evenly distributed in photon frequency. Expressing the terms of Eq. (9) in convenient units we may write the number of detected photons in a given Cherenkov detector as

$$N_{\text{detected}} = N_0 \cdot L(\text{cm}) \cdot \sin^2\theta, \tag{10}$$

where

$$N_0 = 370\ \text{cm}^{-1}\,\text{eV}^{-1} \int \epsilon(\hbar\omega)\, d(\hbar\omega). \tag{11}$$

N_0 is here a quality parameter of the counter, expressed in terms of an integral over photon energy $\hbar\omega$ (in eV) of the photon detector efficiency function $\epsilon(\hbar\omega)$.

Using Eq. (10) to calculate the number of emitted Cherenkov photons in the visible photon energy range (setting $\epsilon \equiv 1$ in the wavelength region 4000–7500 Å corresponding to a $\hbar\omega$ range width of about 1.5 eV) for L = 10 cm one obtains the numbers given in Table 1.

The aim of the present notes is to outline the resolution, the optics design criteria and the expected particle-discrimination performance of a recently developed type of Cherenkov detector conceived to measure the Cherenkov angle of charged particles produced at high-energy particle colliders thus allowing for a determination of the mass, and thereby the identity, of these particles. This type of detector will here be called RICH, as abbreviation for Ring-Imaging Cherenkov counters. In a RICH counter the Cherenkov light emitted by a traversing charged particle is imaged onto a position-sensitive single-UV photon detector of time-projection-chamber (TPC) type, thereby allowing for an experimental determination, over a large solid angle, of the Cherenkov angles for several secondary particles simultaneously [3].

A RICH counter should have as high Cherenkov-angular resolution and as high photon yield as possible, thereby maximizing the useful velocity range over which a mass determination with satisfactory resolution can be made. The counter should furthermore be adaptable to different geometrical configurations and have as small radial extension and as low matter density as possible in order to keep the detector dimensions as small as possible and to minimize secondary particle interactions. Below we will discuss the possibilities and limitations of the RICH technique along these lines.

2. DETECTOR OPTICS AND CHERENKOV ANGLE RECONSTRUCTION

If the light emission per unit track-length from a charged particle travelling in a given radiator medium [see Eq. (10)] is sufficiently large it may be possible to determine the Cherenkov angle with satisfactory precision by measuring the light emitted from a thin layer of radiator by simply projecting the light onto a photon-detector surface at some distance as illustrated in Fig. 2. This scheme is usually practicable when using dense radiators such as liquids. The ultimate geometrical resolution in Cherenkov angle of this method is limited by the finite value of the ratio of the radiator-layer width d to the lever-arm length ℓ.

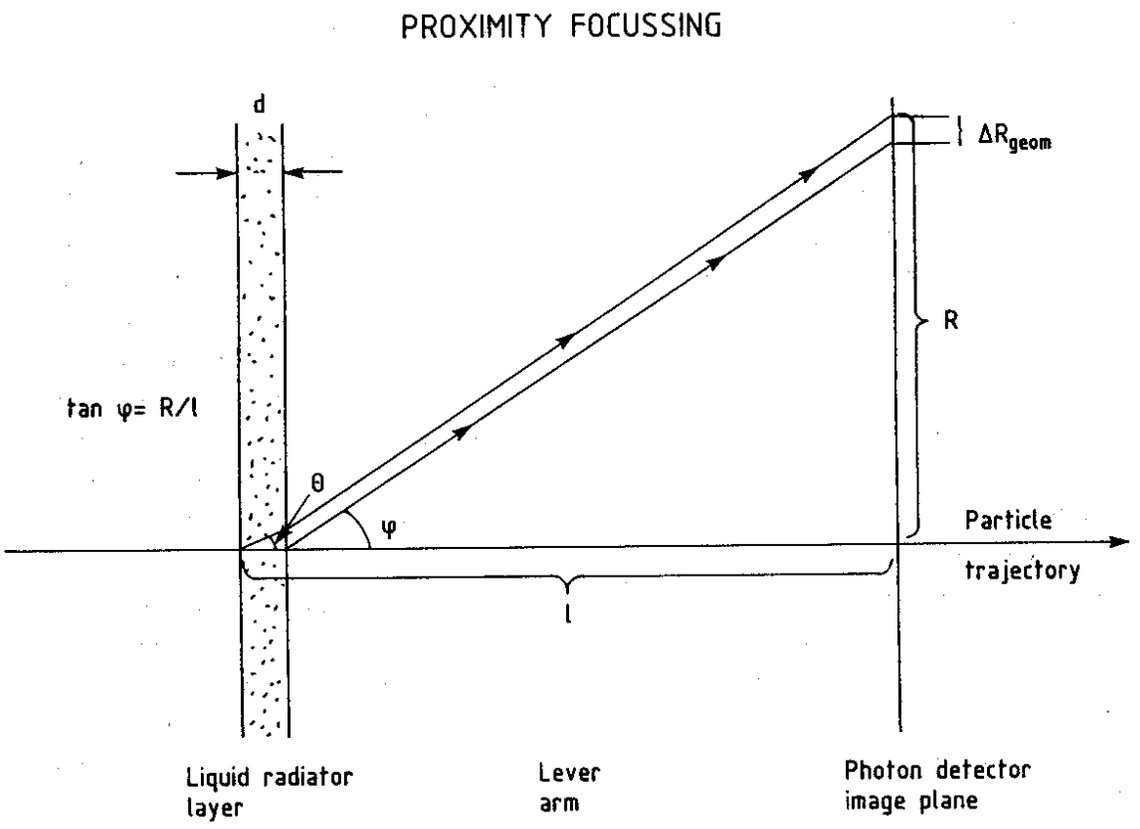

Fig. 2 Determination of the Cherenkov angle by letting the light emitted from a thin liquid radiator layer be projected onto a photon-detector surface ('proximity focussing' [7]).

If, on the other hand, the light emission per unit length of radiator medium is low, as it is in gases, the radiator length has to be maximized. In this case the light has to be focused to retain a satisfactory geometric angular resolution. Cherenkov light is emitted at constant polar angle around the particle trajectory. Therefore, if the trajectory is rectilinear the light is parallel in any given azimuthal plane, and if reflected by a concave spherical mirror the light will focus to a point halfway between the mirror surface and its centre of curvature as illustrated in Fig. 3. Note however that this focusing condition is only valid for small values of θ. For larger angles the photon rays are no longer central and the focal point varies with the location of the point of emission along the particle trajectory. Non-central photon rays are also obtained even in the case of small θ if the particle trajectory does not pass through the centre of curvature of the mirror. The displacement of the focus for non-central photon rays is illustrated by the so-called caustic curve shown in Fig. 4. The deviation of the light from non-central incidence leads to geometrical aberrations in the system, limiting the angular resolution.

The photon acceptance of a RICH counter is maximized if the photon detector covers the light image for all azimuthal angles around the particle trajectory. If so, the image obtained in the photon-detector plane is ring-shaped. The ring is, however, perfectly circular only for particles incident along the optical axis of the detector—in all other cases the image is more or less ellipsoid. For inclined particles in liquid radiators part of the azimuthal acceptance may be lost due to total internal reflection of the Cherenkov light at the inner surface of the liquid and the images are in such cases not even rings but open paraboloids.

To facilitate the reconstruction of the Cherenkov angle the coordinates of the trajectory of the radiating particle must also be measured. A light ray is traced from the location of each detected photon back to the location of the midpoint of the particle trajectory (in the case of a focusing counter after reflection in the mirror) and the Cherenkov angle of the individual photon is calculated as the angle of the reconstructed ray with the particle trajectory. In the case of a liquid radiator it is also of importance to take into account the refraction of the light-ray in the downstream liquid boundary. Double refraction in windows should also be included.

Note that in the case of a focusing counter parallel tracks will, to the first order of approximation, give ring-images with coinciding centres. The position of a Cherenkov ring in a focusing counter thus depends to first order only on the direction of the track and not on its location.

The Cherenkov angle for the particle is calculated as the (possibly weighted) mean-value of the angles reconstructed from the detected photons. The amount of background photons from nearby tracks or other sources can be minimized by selecting only those photons that have a reconstructed angle that falls within 2 or 3 standard deviations from the observed peak value. Alternatively, knowing the momentum of the particle the location of the images of the Cherenkov photons can be predicted assuming the radiating particle to have the mass of either e, μ, π, K, or p. It is then possible to test which of these image locations that best fits with the actually observed location of the photons (the number of

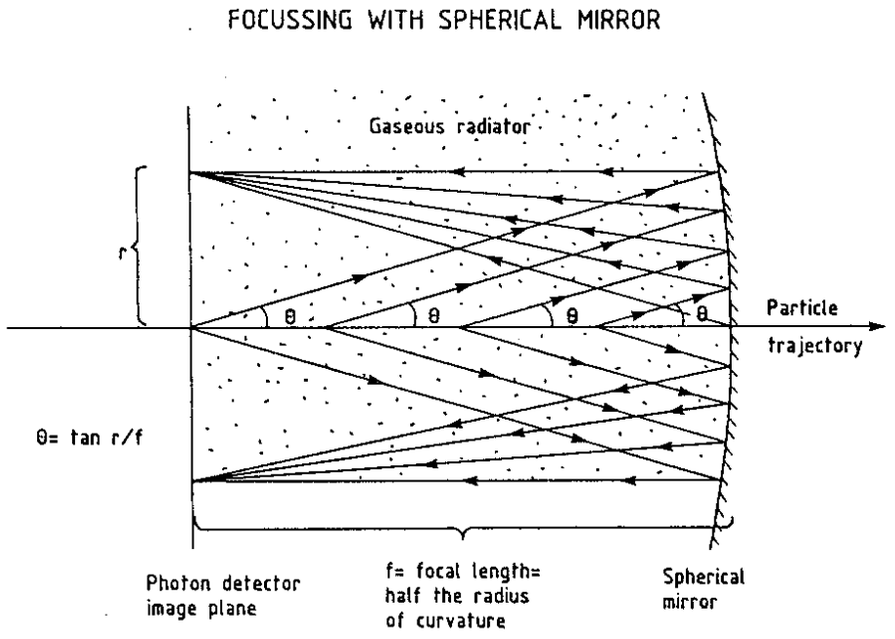

Fig. 3 Determination of the Cherenkov angle by letting the light emitted in a gaseous radiator be focalized by a spherical mirror onto a photon-detector surface.

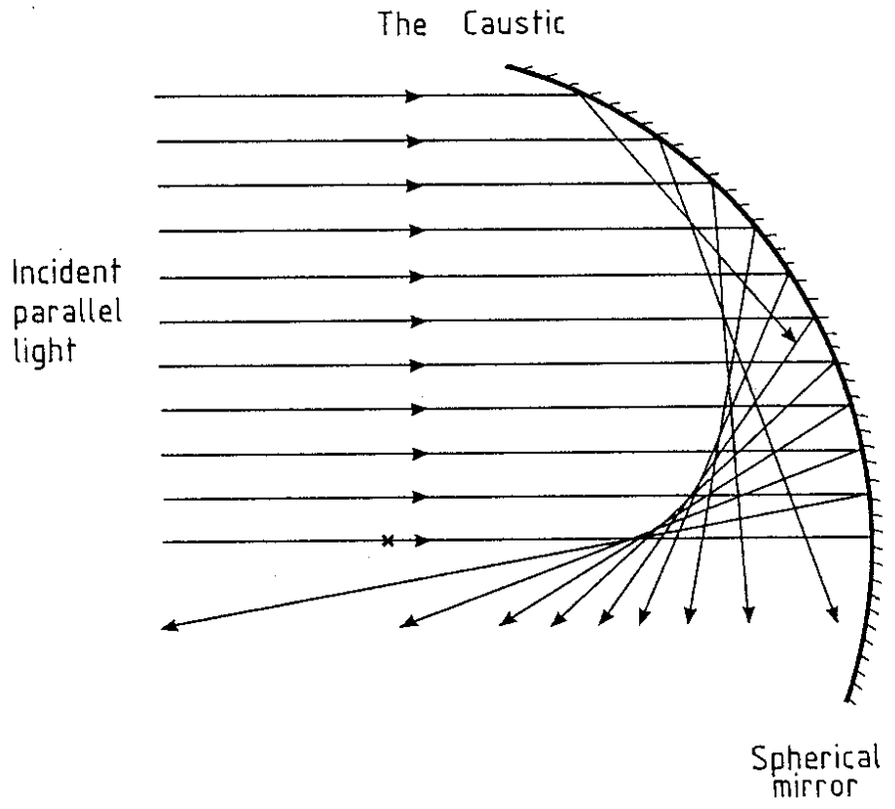

Fig. 4 The so-called caustic curve which shows how the position of the focus for parallel light reflected by a sperical mirror depends on the impact parameter of the light. The center of curvature of the mirror is indicated with a cross. (The caustic can be straightforwardly observed in sunlight, e.g. inside a wedding-ring placed on a flat surface or in a filled coffee cup).

photons falling within 2 or 3 standard deviations from each expected image can be identified and a χ^2 probability for each case evaluated).

Once the Cherenkov angle has been determined the mass of the radiating particle can be calculated provided that also the momentum of the particle has been measured. Contracting Eqs. (4) and (5) we obtain

$$m = p\sqrt{n^2 \cos^2\theta - 1} \tag{12}$$

As the mass ratios of e, π, K, and p (but not μ/π) are relatively large the mass determination can be used to reliably identify any of these particles provided that the standard error in mass is not more than say, for example, $\sigma_m/m = 15\%$. Since m is proportional to p, the momentum resolution required for satisfactory particle identification is then of the same order, i.e. $\sigma_p/p \simeq 15\%$. The requirements on σ_θ/θ are discussed in sections 3 and 4.

3. ANGULAR RESOLUTION AND DESIGN OF COUNTERS WITH GASEOUS RADIATOR

The values of the refractive index minus one $(n - 1)$ and the Cherenkov angle (θ) are both small compared to unity for gaseous radiators. This is, on the other hand, not the case for liquid and solid radiators (see Table 1). In the expressions involving the two quantities mentioned it is therefore possible to make simplifying approximations when dealing with gaseous radiators. Conversely these approximations cannot be used for liquid or solid radiators.

In particular, Eqs. (7) and (8) can be simplified in the following way when θ and $n - 1$ are small.

$$\theta_{max} \simeq \sin\theta_{max} = \sqrt{1 - \cos^2\theta_{max}} = \sqrt{1 - 1/n^2} \simeq \sqrt{2(n-1)} \tag{13}$$

$$\gamma_{threshold} = 1/\sqrt{1 - 1/n^2} \approx 1/\sqrt{(n^2 - 1)} \approx 1/\sqrt{2(n-1)}\,. \tag{14}$$

These approximations do not entail relative errors in θ_{max} or $\gamma_{threshold}$ exceeding 2×10^{-3} for gaseous radiations $[(n - 1) < 2 \times 10^{-3}]$. We have thus obtained

$$\theta_{max} \approx \sqrt{2(n-1)} = 1/\gamma_{threshold}. \tag{15}$$

Let us define a normalized Cherenkov angle θ_{norm} and a normalized Lorenz velocity γ_{norm}, respectively, as

$$\theta_{norm} = \theta/\theta_{max} = \theta/\sqrt{2(n-1)} \tag{16}$$

$$\gamma_{norm} = \gamma/\gamma_{threshold} = \gamma \cdot \sqrt{2(n-1)}\,. \tag{17}$$

Inserting these quantities in Eq. (6) we obtain the following simplified expression [4];

$$\theta_{norm} = \sqrt{1 - 1/\gamma^2_{norm}}. \tag{18}$$

The interesting feature of this expression is, besides its formal simplicity, that it is invariant in the refractive index n. The values of n − 1 for different gases at NTP span several orders of magnitude (see Table 1). The conclusions we will draw from Eq. (18) will nonetheless be equally valid for all gases since the refractive index does not appear in the formula.

Figure 5 shows a plot of relation (18) illustrating how the Cherenkov angle grows very rapidly from zero just above threshold velocity and how it approaches asymptotically its maximum value from below. For values of γ_{norm} large relative to unity we see that θ_{norm} approaches its maximum value of 1 as

$$1 - \theta_{norm} = 1 - \sqrt{1 - 1/\gamma^2_{norm}} \approx 1/(2 \cdot \gamma^2_{norm}), \tag{19}$$

i.e. as half the inverse square of γ_{norm}.

3.1 Angular resolution and particle discrimination

As already discussed in the Introduction, any photon detector will have a certain range $\hbar\omega_1 - \hbar\omega_2$ in photon energy over which it is sensitive (e.g. for the eye $\hbar\omega_1 \approx 3.1$ eV and $\hbar\omega_2 \approx 1.65$ eV). As, in general, the refractive index in a dielectric varies with $\hbar\omega$ this leads to a spread in the observed Cherenkov angle which is not related to the velocity of the radiating particle but to the energy of the particular Cherenkov-photon registered [see formula (6)]. This spread in θ, related to the photon energy spread through the variation in n, is called chromatic aberration. As the photon detectors we discuss here do not measure the individual energy of each photon registered there is no way of correcting for this type of aberration in a wide aperture counter. (As opposed to the case of small aperture counters, for which chromaticity-correcting lenses may be used to reduce the aberration). The angular error in a RICH counter can, therefore, not be smaller than the angular spread caused by chromatic aberration.

The angular resolution of a RICH counter is only of critical interest at high values of γ, where the relative variation in θ is small. In order to obtain the variation of θ with n we may therefore differentiate expression (15) with regard to n

$$\partial\theta/\partial n \approx \partial\theta_{max}/\partial n \approx \partial\,[\sqrt{2(n-1)}]/\partial n = 1/\sqrt{2(n-1)} \tag{20}$$

$$\rightarrow (\Delta\theta/\theta)^{chrom} = \tfrac{1}{2} \cdot \Delta n/(n-1)\,, \tag{21}$$

from which we conclude that the relative spread in Cherenkov angle for a gaseous radiator is equal to half the relative spread in refractive index.

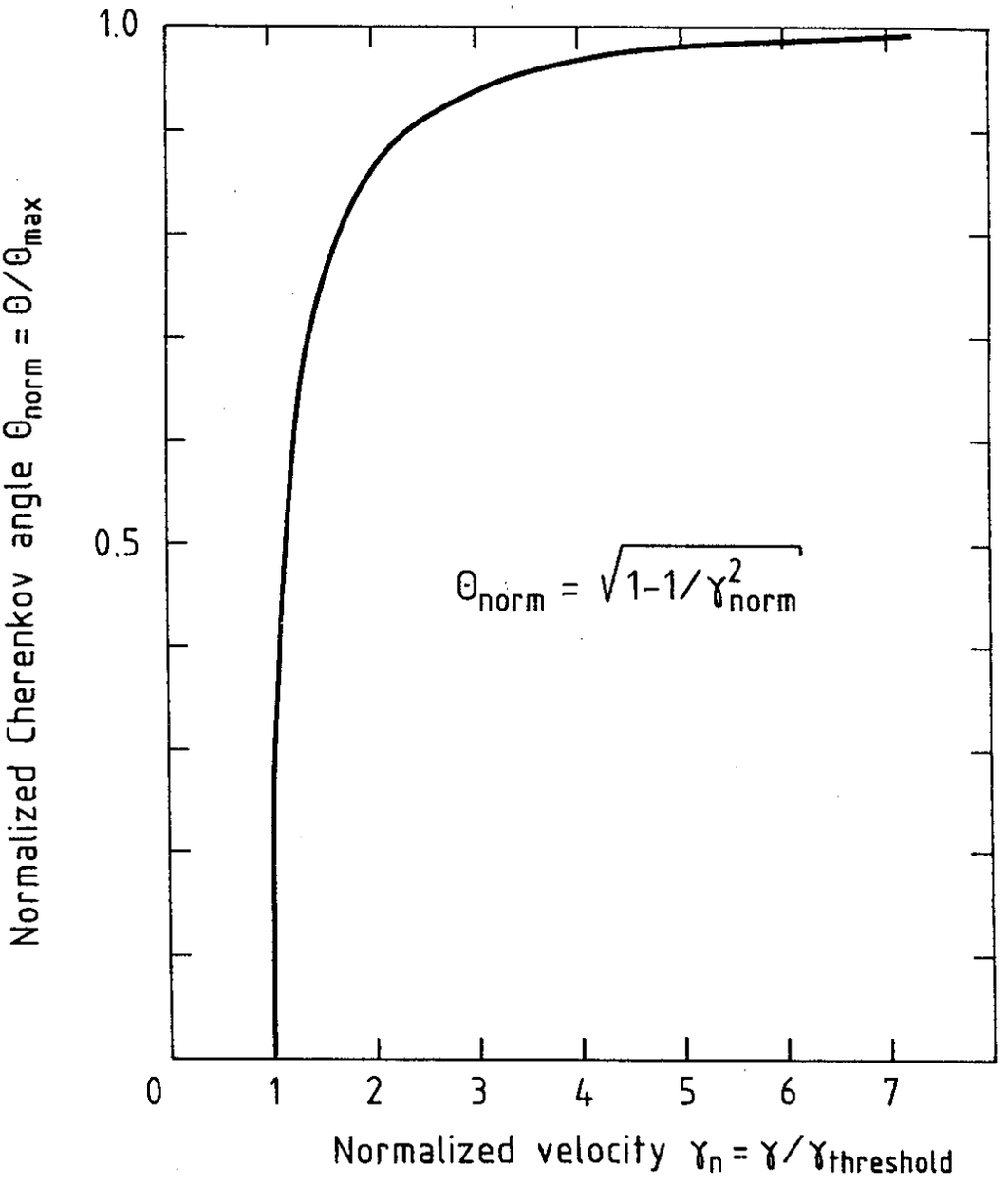

Fig. 5 Plot of Eq. (18) showing how the normalized Cherenkov angle θ_{norm} grows from zero at normalized Lorenz velocity $\gamma_{norm} = 1$ up towards the maximum value $\theta_{norm} = 1$ at large velocities.

Let us now compare the chromatic spread in Cherenkov angle (21) with the deviation $1 - \theta_{norm}$ of the Cherenkov angle from its saturated value (19). Clearly, above the γ_{norm} value for which $\Delta\theta^{chrom}_{norm} > 1 - \theta_{norm}$, it is no longer possible to derive a precise value for γ from a measurement of θ_{norm}. This upper limit in γ_{norm} defined here as γ^{max}_{norm}, is obtained from expressions (19) and (21) as

$$1/(2\cdot\gamma^2_{norm}) = \tfrac{1}{2}\,\Delta n/(n-1) \rightarrow \gamma^{max}_{norm} = \sqrt{(n-1)/\Delta n} = 1/\sqrt{\Delta n_{norm}}\,. \qquad (22)$$

Since the lower limit in velocity for measurement of γ_{norm} by definition is at the threshold, i.e. $\gamma^{min}_{norm} = 1$, the result (22) implies that the dynamical range in γ, defined as $\gamma^{max}/\gamma^{min}$, is equal to the inverse square root of the relative dispersion $\Delta n_{norm} = \Delta n/(n-1)$ in refractive index.

According to expression (14)

$$\gamma^{min} = 1/\sqrt{2(n-1)}\,, \qquad (23)$$

from which it follows that

$$\gamma^{max} = \gamma^{max}_{norm}\cdot\gamma^{min} = [\sqrt{(n-1)}/\Delta n]\cdot[1/\sqrt{2(n-1)}] = 1/\sqrt{2\Delta n} \qquad (24)$$

The upper (lower) limit in γ is thus equal to the inverse square root of twice the absolute dispersion (the residue) of the refractive index.

We will now use these results to evaluate up to what total-energy E two particles of mass m_a and m_b can be separated on the basis of a measurement of θ under the idealized conditions that the chromatic dispersion is the only source of error in θ and that the error in the E measurement is negligible. We thus define that the particles as separated when their corresponding Cherenkov angles differ by $\Delta\theta^{chrom}$.

Given

$$\gamma_a = E/m_a$$
$$\gamma_b = E/m_b$$
$$m_b < m_a$$

we obtain using Eqs. (14) and (19)

$$\theta_{norm,a} - \theta_{norm,b} = \tfrac{1}{2}[m_a/E\sqrt{2(n-1)}]^2 - \tfrac{1}{2}[m_b/E\sqrt{2(n-1)}]^2$$

This difference $\theta_{norm,a} - \theta_{norm,b}$ is equal to the relative angular chromatic dispersion of Eq. (21) when

$$\tfrac{1}{2}\cdot(m_a^2 - m_b^2)/E^2\cdot 2(n-1) = \tfrac{1}{2}\cdot\Delta n/(n-1) \qquad \rightarrow$$

$$E^{a/b}_{max} = \sqrt{m_a^2 - m_b^2}/\sqrt{2\Delta n} = \gamma^{max}\sqrt{m_a^2 - m_b^2}\,. \qquad (25)$$

Table 2

For each of the eleven listed radiator gases are given the refractive index at 7 eV photon energy (177 nm), the threshold velocity, the lower energy limits for π/K and K/p separation, the absolute full-width chromatic dispersion in the range 6.5–7.5 eV, the upper velocity limit imposed by chromatic dispersion, the upper energy limits for π/K and K/p separation, the relative chromatic dispersion in the refractive index and the radiator length required to obtain 15 photons in a $N_0 = 80\ cm^{-1}$ counter.

Radiator gas	$(n-1)\times 10^6$ 7 eV	γ_{th}	$E_{min}^{\pi/K}$ (GeV)	$E_{min}^{K/p}$ (GeV)	$\Delta n \times 10^6$ 6.5–7.5 eV	γ_{max}	$E_{max}^{\pi/K}$ (GeV)	$E_{max}^{K/p}$ (GeV)	$\Delta n/(n-1)$	$\gamma_{max}/\gamma_{min}$	$L_{N_0=80}^{15\ photons}$ (m)
He	33	123	17	60	0.8	790	370	630	2.4%	6.4	28
Ne	64	88	12	43	1.6	560	260	450	2.5%	6.3	15
Ar	300	41	5.7	20	21	155	73	125	7%	3.8	3.1
CH_4	510	31	4.4	15.3	49	100	48	81	9.6%	3.2	1.8
C_2H_2	898	24	3.3	11.6	90	75	35	60	10.0%	3.2	1.0
C_4H_{10}	1500	18	2.6	8.9	160	56	26	45	10.7%	3.1	0.63
CF_4	488	32	4.5	16.6	10	225	105	180	2.0%	7.0	1.9
C_2F_6	793	25	3.5	12.3	23	150	69	120	2.9%	5.9	1.2
C_4F_{10}	1510	18	2.5	8.9	53	97	46	78	3.5%	5.3	0.62
C_5F_{12}*	1750	17	2.4	8.3	51	100	47	79	2.9%	5.9	0.54
C_6F_{14}*	1950	16	2.3	7.8	59	92	43	73	3.0%	5.7	0.48

* liquid at NTP

This is the upper limit in particle total energy for discrimination between particles a and b. Assuming $m_b < m_a$ the corresponding lower limit is simply obtained as the energy below which none of the particles radiates

$$E_{min}^{a/b} \equiv m_b \gamma_{threshold} = m_b \sqrt{2(n-1)}\,. \tag{26}$$

In Table 2 we have listed the values of $n - 1$ and Δn for three noble gases, three hydrocarbon gases, and five fluorocarbon (freon) gases (at NTP except C_5F_{12} and C_6F_{14} which are not gases at NTP). The photon energy range has been assumed to be in the far ultraviolet region 6.5–7.5 eV (wavelength 1650–1900 Å). For each gas γ_{min}, $E_{min}^{\pi/K}$, $E_{min}^{K/p}$, γ_{max}, $E_{max}^{\pi/K}$, $E_{max}^{K/p}$, $\Delta n/(n-1)$, the dynamical range $\gamma_{max}/\gamma_{min}$ and the length of radiator gas required to detect 15 photons in a counter of quality parameter $N_0 = 80\ cm^{-1}$. The range in γ and E for each gas has also been illustrated in Fig. 6.

As seen, the noble gases and the freons have about the same relative dispersion in n (of the order of 3%), whereas the hydrocarbons are about three time more dispersive. If one wants to reach high values in n, keeping $\Delta n/(n-1)$ low, the heavy freons are to be preferred (note that C_5F_{12} and C_6F_{14} are liquids boiling at 30°C and 57°C respectively—the values of the refractive indices given are valid for the gaseous phase at 1 atm just above the boiling point).

3.2 Other sources of error and counter design

In addition to the chromatic dispersion there are, of course, other sources of error in the measured Cherenkov angle. These other sources are, however, such that by a careful design of the detector the chromatic error will remain the dominant error. We will study below how this condition actually dictates the design of a RICH detector

3.2.1 Geometric aberration

As already noted, the focusing of parallel rays in a spherical mirror is exact only in the case when the light ray passes through the centre of curvature of the mirror. As the Cherenkov light makes an angle with the particle trajectory there will be some geometric aberration in the focusing even if the particle trajectory passes through the centre of curvature of the mirror (the particle track has zero impact parameter). If, in addition, the particle track passes the centre of curvature of the mirror at some distance, i.e. at a non-zero value of the impact parameter $x = \delta/R$ (where δ = the distance and R = radius of curvature of the mirror) the geometric aberration will increase. Evaluating the geometrical aberration error as a function of x for Cherenkov light focused by a spherical mirror [5] one obtains for the full width of the relative angular spread

$$(\Delta\theta/\theta)_{geom} = (n-1)\cdot\sqrt{3} \oplus (\sqrt{42\,(n-1)}/7)\cdot x \oplus x^2 \oplus \ldots, \tag{27}$$

where $\oplus$ means addition in quadrature. From Eq. (27) we may conclude that at $x = 0$, $(\Delta\theta/\theta)_{geom} = (n-1)\sqrt{3}$ and that for large values of x $(\Delta\theta/\theta)_{geom}$ increases like x^2

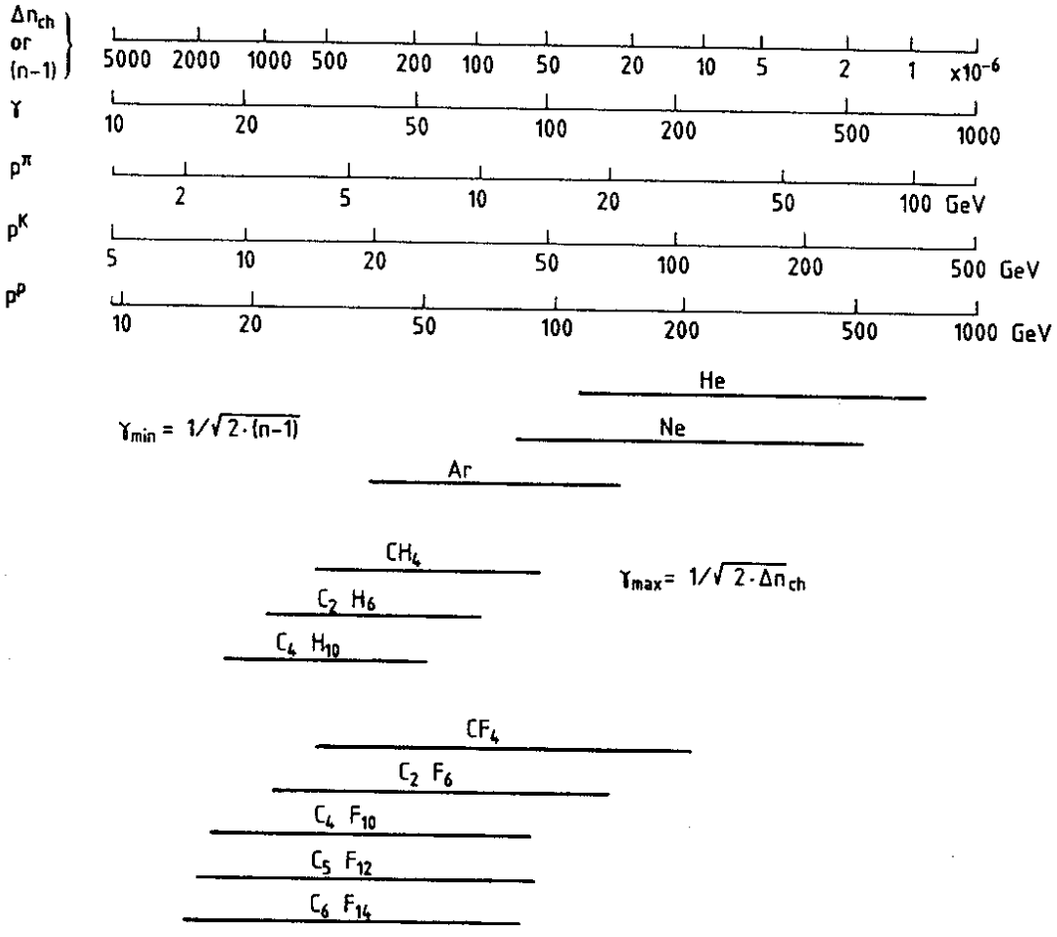

Fig. 6 Graph illustrating the ranges within which velocity measurements can be made using a gaseous-radiator RICH counter with different gasses. The lower limit is set by the absolute threshold $\gamma^{min} = 1/\sqrt{2(n-1)}$ and the upper limit by chromatic dispersion for photon energies 7 ± 0.5 eV, $\gamma^{max} = 1/\sqrt{2\Delta n}$. There are scales indicating the momentum for π, K and p. (The data of this graph is listed in Table 2).

(the x^2 term dominates over the x term above $x = 0.03$ for $n \leq 1.002$). Figure 7 shows a plot of $(\Delta\theta/\theta)_{geom}$ versus x for $n = 1.002$.

In order to satisfy the requirement that $(\Delta\theta/\theta)_{geom} < (\Delta\theta/\theta)_{chrom}$ an upper limit on x must be imposed. In the optical scheme originally proposed [6] for wide-aperture RICH counters the centre of curvature of the mirror coincides with the point of emission of particles (see Fig. 8, spherical RICH) and x is zero for all directions of particle emission (at least in the case of zero magnetic field). For a RICH counter at a collider that should cover the full solid angle this implies a spherical geometry with the radius of the detector sphere exactly half that of the mirror sphere. Such a geometry imposes severe restrictions on the space available to other detectors in the experiment and on their geometry. In order to obtain a more flexible layout the sphere may, however, be cut up into small spherical sectors, called cupolas (see Fig. 8), which can be laid out in arrays that fit the geometry of the overall experimental layout. The centre of curvature of a cupola mirror need not at all coincide with the centre of emission of particles. It is sufficient that the aperture of each cupola be limited such that the geometrical aberrations are small [7]. Choosing for the discussion a radiator for which $[\Delta n/(n-1)]_{chrom} = 4\%$ (ref. Table 2) the relative angular resolution is (Eq. 21) $(\Delta\theta/\theta)_{chrom} = 2\%$. For $(\Delta\theta/\theta)_{geom}$ to be smaller than $(\Delta\theta/\theta)_{chrom}$. Eq. (27) implies the requirement $x < 0.14$.

The apertures of the cupola should thus in this case be such that the impact parameter x for all tracks is smaller than 0.14. Figure 9 shows an early working drawing of a spherical-mirror cupola-array layout from the discussions that led to the conception of the DELPHI RICH counters at LEP.

In some cases it is preferable to use paraboloid mirrors, for example when the impact parameter is large but the angular spread of the particle trajectories is small. This condition is fulfilled, for example in the Barrel RICH of the DELPHI detector, where paraboloid mirrors are used in the final design. Other shapes of the mirrors for example ellipsoid could be optimal in certain cases.

3.2.2 Photon positioning errors

The position resolution Δr_{xy} in the image plane of the photon detector should be such that (r = ring radius)

$$(\Delta r/r)_{xy} < (\Delta\theta/\theta)_{chrom}. \tag{28}$$

Choosing, somewhat arbitrarily, as example $\theta = 60$ mrad and $f = 1000$ mm (i.e. $r = 60$ mm) this implies $\Delta r < 1.2$ mm if $(\Delta\theta/\theta)_{chrom} = 2\%$. The photon detector should thus, in this case, have a position resolution of the order of 1 mm or better in order for the chromatic error to dominate.

Ideally the lateral position of all photons should be measured exactly in the focal surface. However, this is not possible in practice. A spread Δz in longitudinal coordinate (transverse to the focal plane) of the point at which the lateral coordinates x and y of the photon track is measured will tend to increase the relative uncertainty in the measured

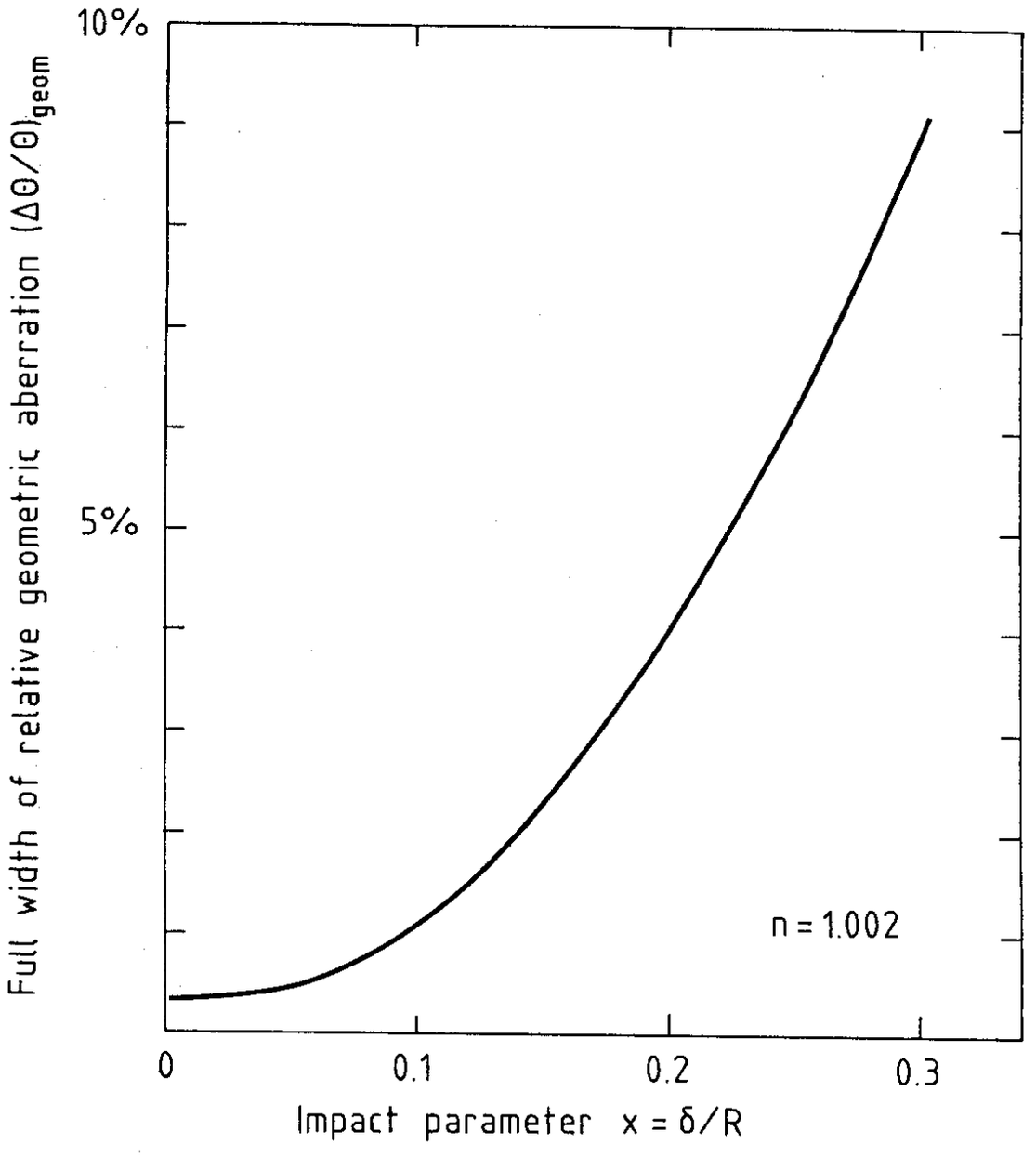

Fig. 7. Graph showing the relation between the relative full-width of the geometric aberration $(\Delta\theta/\theta)_{geom}$ as function of the impact parameter x of the particle trajectory in a RICH counter (radiator refractive index is 1.002).

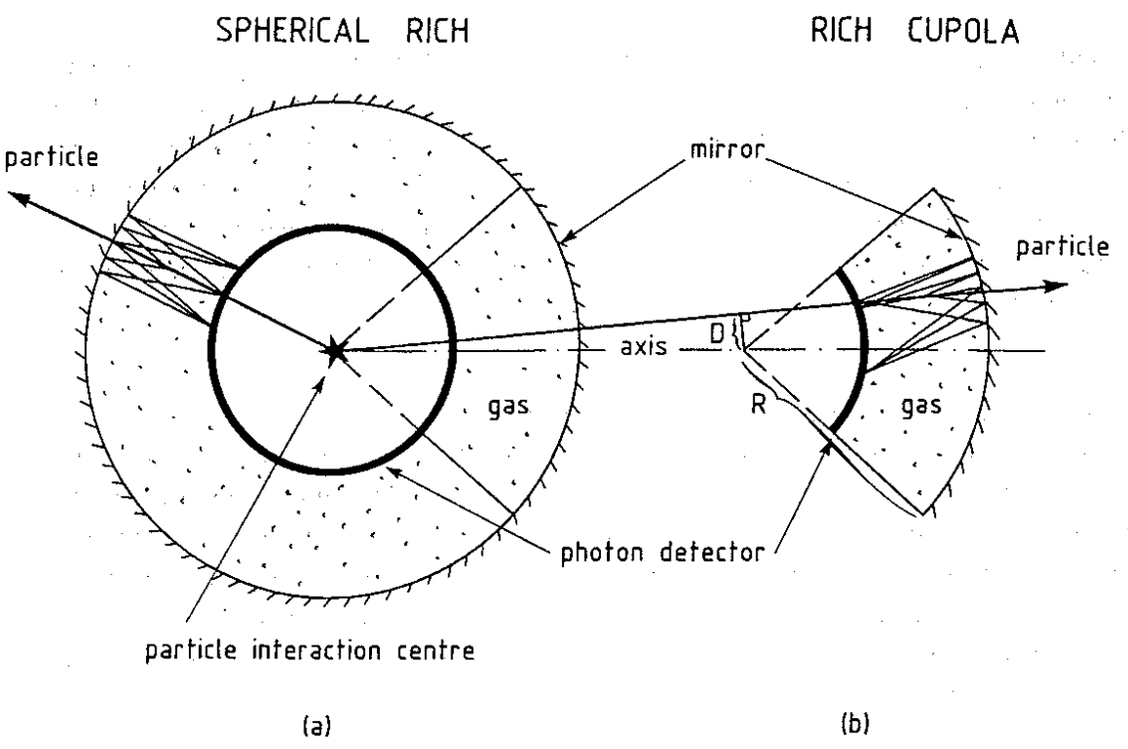

Fig. 8. The optics of the originally proposed spherical RICH counter [6] and that of a so-called 'cupola' RICH counter [7].

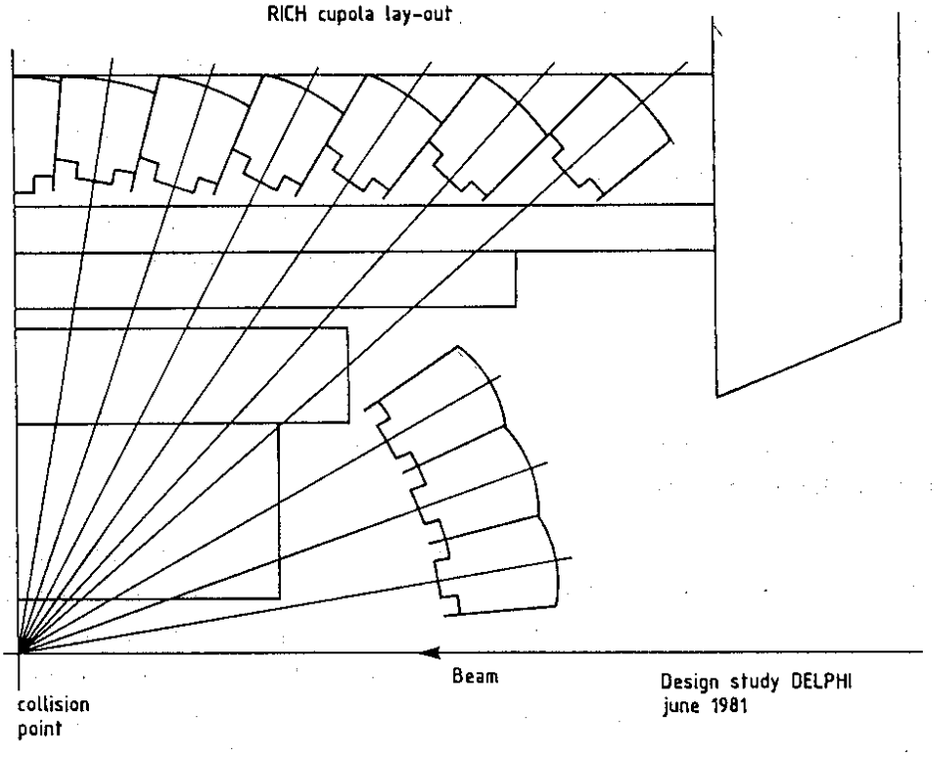

Fig. 9. Early working-drawing of a spherical-mirror cupola-array from the discussions that led to the conception of the DELPHI RICH counters.

Cherenkov angle. For this spread in θ to be smaller than that caused by chromatic aberration is required that $\Delta z < f \cdot (\Delta\theta/\theta)_{chrom}$ in case of perpendicular incidence of the light on the photon detector. However, if $x \neq 0$, the light will in general hit the photon detector at an angle α, which in practical cases can be considerable. In such cases the image aberration is systematic and can be corrected for provided that the depth coordinate z is measured with sufficient accuracy [the accuracy required for z depends on α, $\Delta z < f \cdot (\Delta\theta_{chrom}/\alpha)$].

3.2.3 Magnetic field and multiple Coulomb scattering

As already discussed, in order to use the measurement of the velocity γ to identify particles, the momentum of the particle must also be known. This implies, in practice, that a magnetic spectrometer must be used. If the Cherenkov counters have to be placed in the magnetic field of the spectrometer the particle track will be bent and the image distorted. The effect on the image is illustrated in Fig. 10. The displacement $\Delta\theta$ in angle for a particle of momentum p traversing a radiator of length d in a magnetic field with a component B_T perpendicularly to the particle trajectory is

$$\Delta\theta = 0.3\, B_T d/p\,. \tag{29}$$

Averaging the angular smear around the ring reduces $\Delta\theta$ by a factor $2/\pi$. As it is at high momenta (where the difference in ring radius for different particles is small) that a high resolution in θ is needed B_T can in practical cases be quite high ($\sim$ 1T) without significantly deteriorating π/K and K/p separation. However, e/π separation may be significantly affected since the π ring approaches the e ring in radius at comparatively much lower momenta.

It should also be noted that the magnetic field in general will affect the operation of the photon detector, possibly changing its position resolution.

Another reason for the particle trajectory not to follow a straight line is multiple Coulomb scattering in the radiator. This effect is, however, in most practical cases of negligible magnitude.

4. ANGULAR RESOLUTION AND DESIGN OF COUNTERS WITH LIQUID RADIATORS

There are several qualitative differences between the case of liquid radiators and that of gaseous radiators. As seen from Table 1, comparing a heavy gas (such as isobutane) with a light liquid (such as freon), the density of emitted photons is more than two orders of magnitude larger and the Cherenkov angle more than one order of magnitude larger in the case of the liquid. These facts are, of course, just reflections of the large step in $(n - 1)$ of more than two orders of magnitude when going from gases to liquids. The consequences are the following.

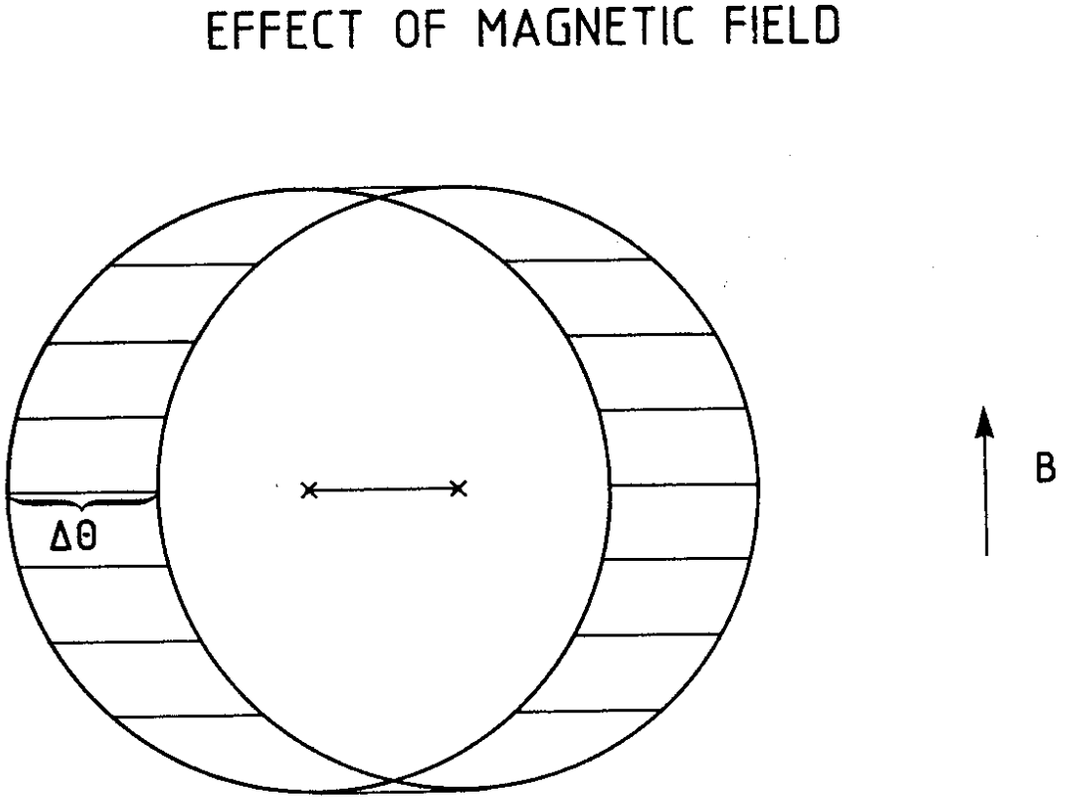

Fig. 10 Illustration of how a Cherenkov ring is smeared if the radiating particle passes through a magnetic field.

i) In view of the high photon density a liquid radiator may be made thin ($\sim$ 1 cm), so that θ can be measured by simple projection without focusing mirrors [7], as already discussed (see Fig. 2).

ii) The large value of θ implies that the small-angle approximation is no longer valid.

iii) The large value of the refractive index implies that refraction of Cherenkov light in the downstream liquid surface has to be taken into account. In particular, under certain conditions the Cherenkov light is subject to total internal reflection.

vi) Finally, the relative range of $(n - 1)$ is much smaller for liquids than for gases. In terms of the ratio $(n_{max} - 1)/(n_{min} - 1)$ the range is about 45 for gases at NTP (see Table 1, $n_{min} = 1.000035$, $n_{max} = 1.00127$) but only 1.8 for liquids ($n_{min} = 1.233$, $n_{max} = 1.41$; for $n > 1.41$ all Cherenkov light is totally internally reflected for particle trajectories normal to the downstream liquid boundary). This implies that it is not possibler to change dramatically the lower velocity limit γ_{min} for particle-discrimination of a liquid-radiator counter by changing the liquid.

With reference to Fig. 2, defining as in the case of gaseous radiators a normalized radius $R_{norm} = R/R_{max}$ and a normalized velocity $\gamma_{norm} = \gamma/\gamma_{threshold}$, we obtain the relation between R_{norm} and γ_{norm} by contraction of the following expressions

$$R_{norm} = \tan\phi/\tan\phi_{max}$$

$$\phi = \arcsin(n \sin\theta) \qquad \text{(Snell's law)} \tag{30}$$

$$\theta = \arccos[1/(n \cdot \sqrt{1 - 1/\gamma^2})] \tag{6}$$

$$\gamma = \gamma_{norm}/\sqrt{1 - 1/n^2} \tag{8}$$

$$\gamma_{norm}^{max} = 1$$

leading to

$$R_{norm} = \frac{\tan[\arcsin(n \sin[\arccos[1/(n \times \sqrt{1 - (1 - 1/n^2)/\gamma_{norm}^2})]])]}{\tan(\arcsin[n \sin[\arccos(1/n)]])} \tag{31}$$

to be compared with the expression obtained for gaseous radiators

$$r_{norm} = \theta_{norm} = \sqrt{1 - 1/\gamma_{norm}^2}\,. \tag{18}$$

In the limit $n \to 1$ Eq. (31) reduces to Eq. (18). Clearly, Eq. (31) does not have the formal simplicity of Eq. (18) and, more importantly, Eq. (31) is *not invariant in n* as is Eq. (18). Therefore, conclusions drawn from Eq. (31) will be different for different liquids (different values of n). The scale-breaking in n is illustrated in Fig. 11, where R_{norm} has been plotted versus γ_{norm} for different values of n between 1.20 and 1.40. When $n \to 1$ the curves tend to

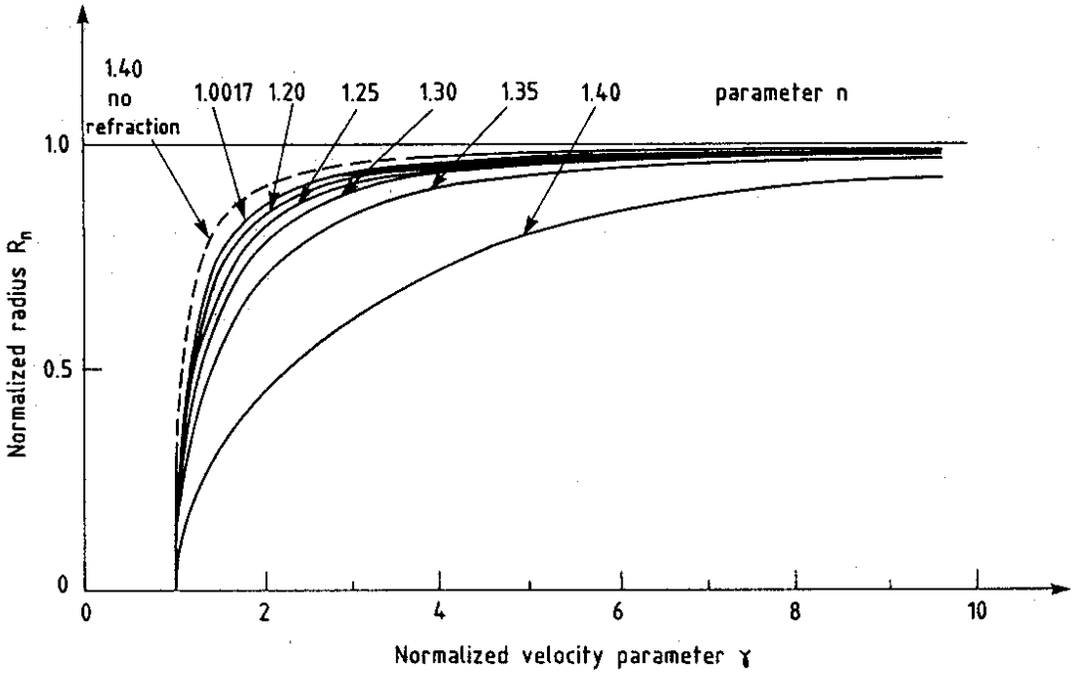

Fig. 11 Plot of Eq. (31) showing the relation between the normalized Cherenkov-ring radius R_{norm} and the normalized velocity γ_{norm} for normal incidence of particles in a proximity focussing liquid-radiator RICH-counter for different values of the refractive index n.

the limiting curve, here labelled n = 1.0017, which, as already stated [relation (18) invariant in n] is valid for all gases. The dashed curve has been calculated for n = 1.40 *not* including the effects of refraction [relation (30)]. The significant difference between this curve and that including refraction for n = 1.40 shows the dominant importance of the refraction as n approaches the limiting value $n = \sqrt{2}$, above which total reflection occurs.

In Fig. 12 R_{norm} has again been plotted, this time as a function of γ ($= \gamma_{norm} \cdot \gamma_{threshold}$). It is apparent from this figure that the available range in threshold velocities is quite limited; $\gamma_{threshold}$ = 1.41 (n = 1.41) to 1.67 (n = 1.25). However, the curve for n = 1.40 seems to stretch over quite a large dynamical range, having a very low threshold and approaching $R_{norm} = 1$ at about the same rate as the curve for n = 1.02. From these considerations alone one would conclude that a liquid with a refractive index just below n = 1.41 would represent an optimal choice. However, as discussed in the following section, chromatic dispersion in the refraction invalidates such a conclusion.

4.1 Angular resolution and particle discrimination

As for a gaseous-radiator counter the ultimate limit in angular resolution is set by the chromatic dispersion of the refractive index. To study the effects of this dispersion for liquid radiators we cannot use the simple Eq. (21), primarily because this formula does not include the additional angular spread introduced through chromatic dispersion in the refraction in the downstream liquid surface and also because of the fact that the small-angle approximation used to derive this formula is no longer valid.

An overriding condition when choosing a radiator is that it be transparent to the photons to be detected. As the TPC-type photon detectors developed so far use tetrakis-(dimethylamine)-ethylene (TMAE) as the photo-ionizing component, only photons of an energy above the photo-ionization threshold of this substance which is 5.4 eV (wavelengths below 230 nm) can be detected. If purified fused quartz is used as window material only light of energy below the transparency threshold of this material, 7.5 eV (165 nm), can be detected. As a consequence, we require a good radiator to have a high transparency over most of the interval 5.4–7.5 eV. This condition is fulfilled for the noble gases and the lighter hydrocarbons and fluorocarbons listed in Table 2. However, we have already mentioned that the hydrocarbons have a larger chromatic dispersion in this photon-energy range as compared to the nobel gases and the fluorocarbons. We could thus obtain satisfactory radiator liquids by liquefying noble gases or fluorocarbons. There are obvious practical advantages of not having to work at low temperature. This in turn implies that the use of liquefied noble gases should be avoided and focuses the choice on the heavy fluorocarbons which are in liquid phase at room temperature. In Table 3 we have listed a series of fluorocarbons with their refractive indecies at 7 eV and the absolute and relative variation in n over the range 6.5–7.5 eV (below 6.5 eV the quantum efficiency of TMAE is quite low). Of these only C_5F_{12} and C_6F_{14} are liquid at room temperature.

From Table 3 we see that the value of $\Delta n/(n - 1)$ is about 3% for the fluorocarbons. Using Eq. (31) we may now explicitly calculate the relative spread in radius $(\Delta R/R)_{chrom}$ for different values of n, assuming a relative full width dispersion in n of $\Delta n/(n - 1) = 3\%$.

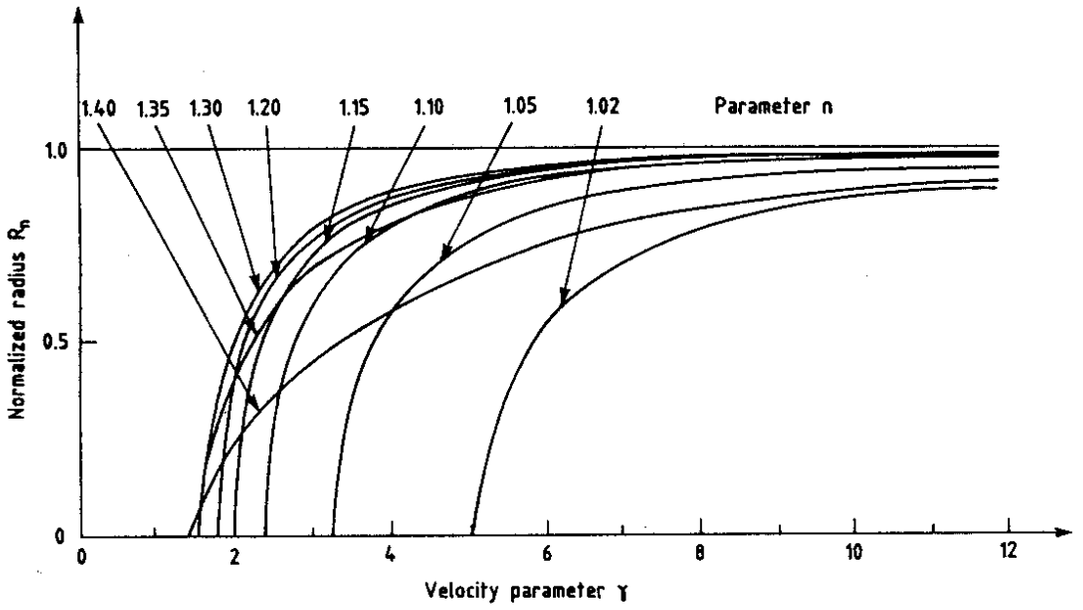

Fig. 12 Plot of the same relation as in Fig. 11 with the difference that the abscissa does not represent the normalized velocity γ_{norm} but the absolute velocity γ (= $\gamma_{norm}\gamma_{threshold}$)

Table 3

For each of the five listed radiator liquids are given the refractive index at 7 eV photon energy (177 nm) and its absolute and relative full-width chromatic dispersion in the range 6.5–7.5 eV. For each radiator the temperature at which the measurement was made is indicated in parenthesis (only the last two are liquids at room temperature).

Radiator liquid	n 7 eV	Δn_{chrom} 6.5–7.5 eV	$\Delta n/(n-1)$
CF_4 (−136 °C)	1.226	0.0047	2.1%
C_2F_6 (− 82 °C)	1.248	0.0075	3.0%
C_4F_{10} (−10 °C)	1.266	0.0102	3.8%
C_5F_{12} (+20 °C)	1.262	0.0080	3.1%
C_6F_{12} (+20 °C)	1.277	0.0093	3.4%

The corresponding curve is shown in Fig. 13. As expected [see formula (21)] $(\Delta R/R)_{chrom}$ tends to $(\frac{1}{2})\cdot\Delta n/(n-1) = 1.5\%$ when n goes to 1. Repeating the calculation without refraction included in the expression for R_{norm}, $(\Delta R/R)_{chrom}$ is equal to 1.5% at all values of n (dashed line in Fig. 13). However, when refraction is included, $(\Delta R/R)_{chrom}$ increases with n and grows rapidly to very large values when n approaches the value $\sqrt{2}$. The actual loci in Fig. 13 for the fluorocarbons in Table 3 have been marked with crosses. For comparison the loci of liquefied noble gases have also been indicated (He, Ne, and Ar). For the two fluorocarbons in Table 3 that are liquids at room temperature $(\Delta R/R)_{chrom} = 4\text{–}5\%$, which is a large increase from the value of 1.6–1.7% [$= (\frac{1}{2})\Delta n/(n-1)$] these media have in gaseous phase. The reason for this increase is to be found in the additional refractive dispersion occurring in the downstream liquid surface.

Let us now evaluate in the same way as in the case of gaseous radiators over what γ-range a measurement of the velocity can be made by comparing the deviation $(1 - R_{norm})$ with the relative chromatic spread $\Delta R_{norm,chrom}$. In Fig. 14 the ratio of these two quantities $(1 - R_{norm})/\Delta R_{norm,chrom}$ has been plotted as a function of γ for a series of different values of n. Throughout, the value assumed for $\Delta n/(n-1)$ is 3% as approximately valid for the fluorocarbons.

From Fig. 14 it is apparent that the γ-value at which $(1 - R_{norm})$ is equal to $\Delta R_{norm,chrom}$ decreases monotonically with increasing n. From this we may conclude that the large dynamical range in the variation of R_{norm} with γ for values of n just below $n = \sqrt{2}$ (see Fig. 12) is counteracted by the strong increase in relative chromatic dispersion $(\Delta R/R)_{chrom}$ when approaching $n = \sqrt{2}$ (shown in Fig. 13). The net result is that if the goal is to measure the velocity to the highest possible value of γ, one should choose the radiator liquid that has the lowest possible value of n (as seen in Fig. 14). Of the liquids in Table 3 C_5F_{12} boils at

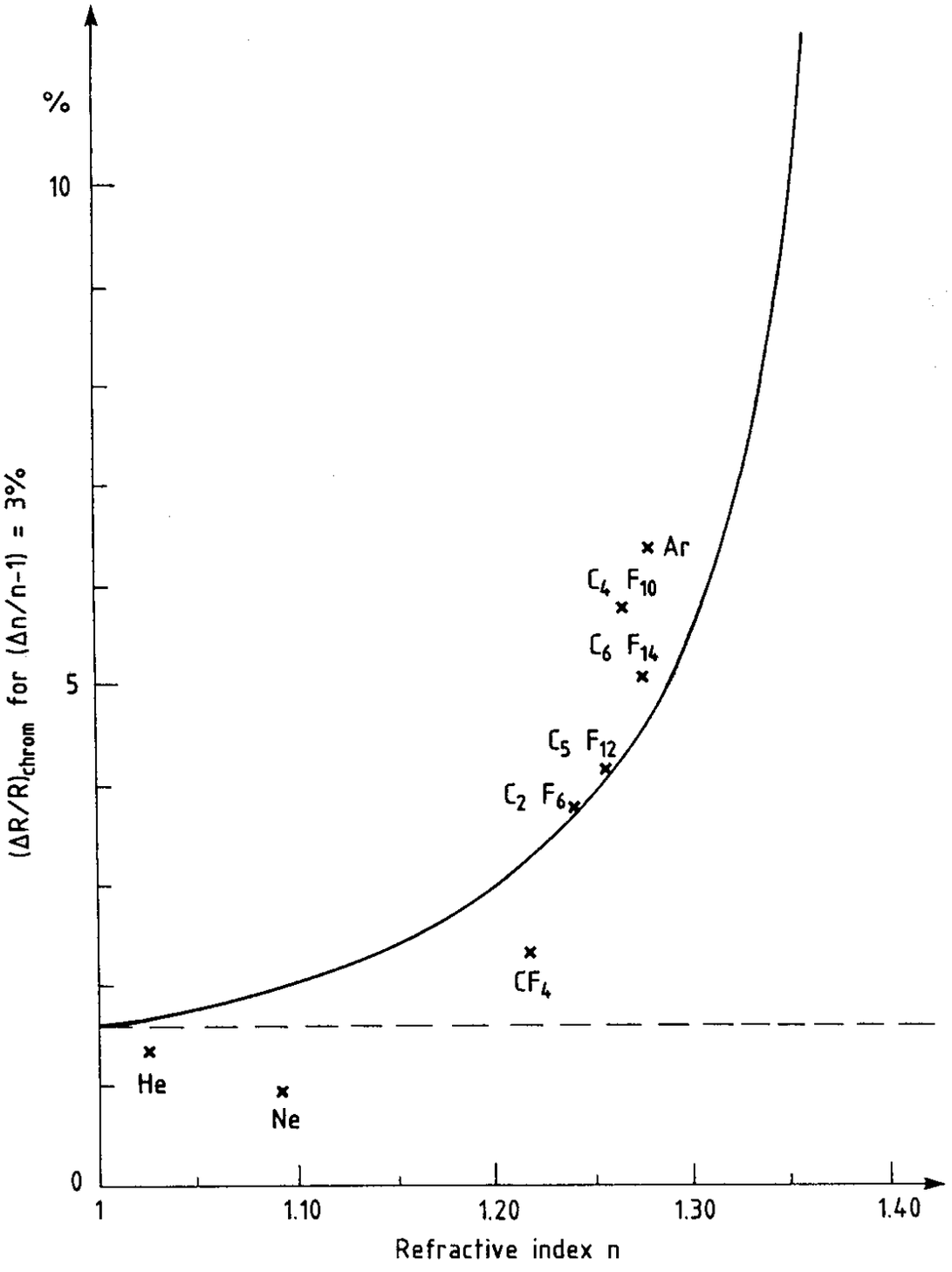

Fig. 13 The relative full-width of chromatic dispersion in Cherenkov-ring radius R in a liquid radiator RICH counter for particle of normal incidence as function of the refractive index, assuming a constant relative full-width dispersion in the refractive index of $\Delta n/(n - 1) = 3\%$. The crosses show the locii for various radiator liquids in the graph. The dashed line shows the dispersion in R if there were to be no refraction in the counter.

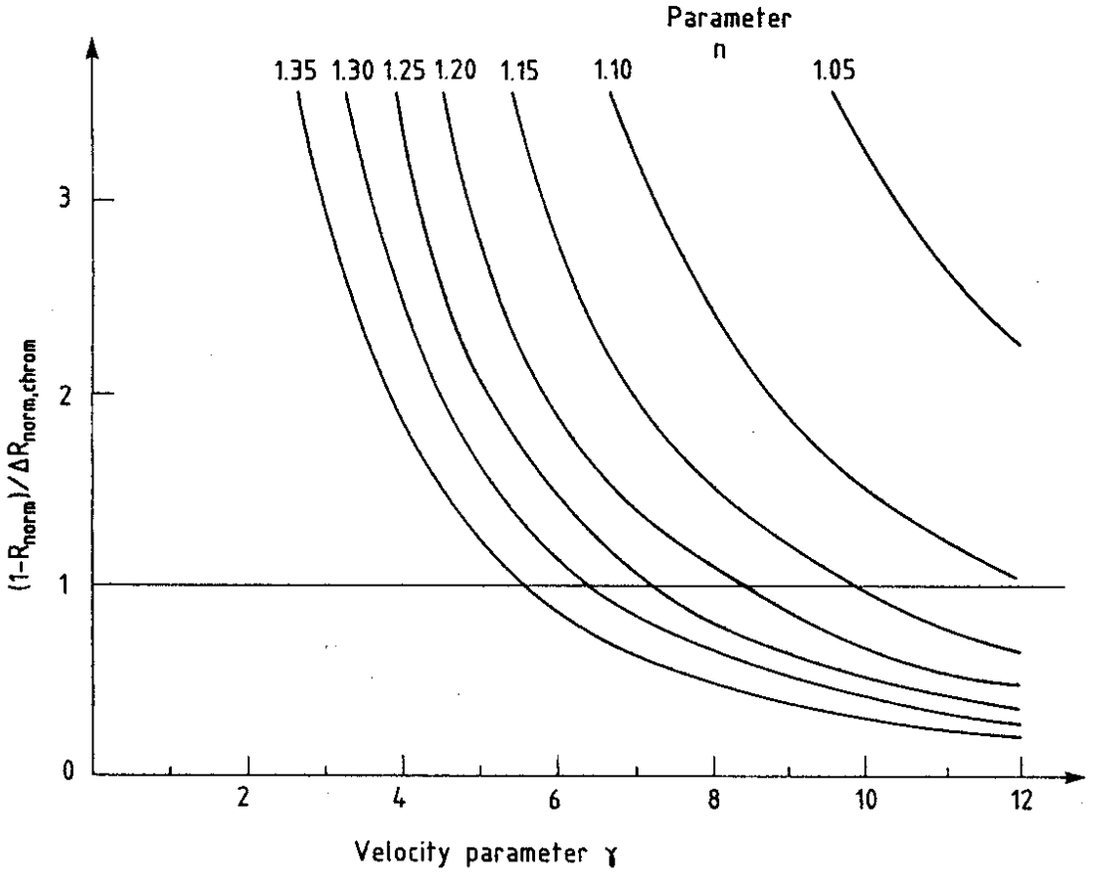

Fig. 14 The ratio between the deviation of the normalized radius R_{norm} from its saturated value 1 and the full width in R_{norm} due to chromatic dispersion as function of velocity in a liquid-radiator RICH counter for different values of the refractive index n.

30° C and C_6F_{14} at 56° C. We will choose C_5F_{12} as an example to evaluate the upper and lower limits in energy for particle discrimination. From Table 3 we have for C_5F_{12}

$$\left.\begin{array}{l} n = 1.262 \\ \text{relation (8)} \end{array}\right\} \gamma_{threshold} = 1.64$$

$$\left.\begin{array}{l} \Delta n/(n-1) = 3.1\% \\ \text{Figure 14} \end{array}\right\} \gamma_{max} = 7.2$$

which implies the following momentum ranges for the three stable, charged hadrons

π	180 GeV/c	to	1000 MeV/c
K	640 GeV/c	to	3500 MeV/c
p	1220 GeV/c	to	6700 MeV/c.

The velocity range for C_5F_{12} is shown together with the velocity ranges for the gaseous radiators (from Fig. 6) in Fig. 15. Assuming that C_5F_{12} is the lightest available UV-transparent liquid at room temperature with low relative chromatic dispersion, then the upper γ limit cannot be increased by choosing other radiator liquids (however, if a cryogenic and/or pressurized liquid-radiator container can be used, this is certainly not true). The lower limit in γ (i.e. $\gamma_{threshold}$) can be lowered to $\gamma = 1.41$, as indicated in Fig. 15, by using a liquid (or solid) with a refractive index just below $n = 1.41$ but only at the price of significantly decreasing the upper limit γ_{max}.

Let us finally note that using the heaviest gaseous radiator an absolute threshold as low as 2.4 GeV/c is obtainable for π mesons (using, for example, C_5F_{12} in gaseous phase—see Table 2). Above 2.4 GeV/c it is thus possible to separate π's and K's using a gaseous-radiator counter alone. Adding, in series, a liquid-radiator counter would allow π/K separation up to 3.5 GeV/c. There is thus an overlap between the two counters which assures continuous π/K separation at momenta from the π momentum threshold in the liquid (180 MeV/c) up to the upper K momentum limit in the gas (47 GeV/c—see Table 2). For K/p separation, on the other hand, the K threshold in the gas is about 8.3 GeV/c, whereas the maximum momentum for protons to be measured in the liquid-radiator counter is 6.7 GeV/c. For the case of K/p separation a combined liquid and gaseous-radiator counter will thus have a region of reduced performance around 7–8 GeV/c. The 'hole' in K/p separation would be reduced if one can find a liquid radiator of even lower n and $\Delta n/(n-1)$ or a gaseous radiator of even higher n than has been discussed here.

4.2 Other sources of error and counter design

As for the gaseous-radiator RICH, the design of a liquid-radiator RICH is dictated by the ambition to reduce the other sources of error in the mesured Cherenkov angle to such an extent that the irreducible chromatic dispersion remains the dominant error source. Choosing C_5F_{12} as radiator liquid we have $(\Delta R/R)_{chrom} \approx 4\%$.

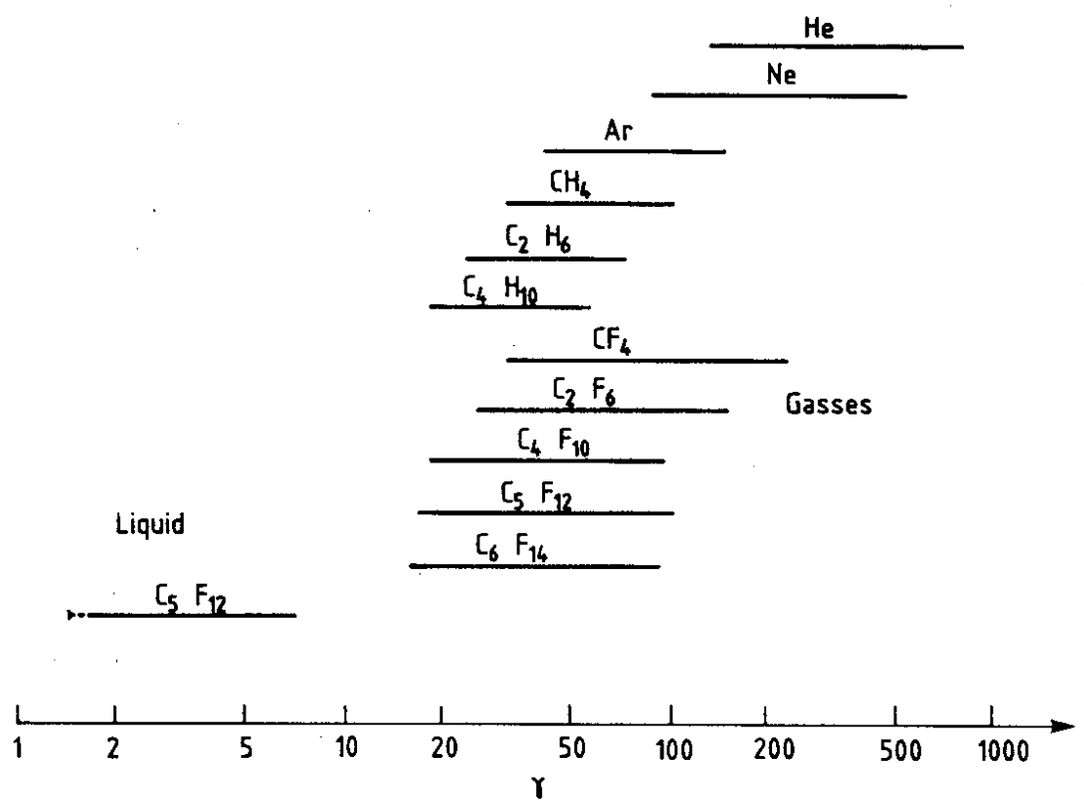

Fig. 15 This graph shows the same velocity-measurement ranges for gaseous radiators as displayed in Fig. 6 and in addition the range corresponding to a liquid-radiator RICH counter with C_5F_{12} as radiator (n = 1.262). The dashed line shows the small extension that is possible towards lower velocities by going to heavier liquids (up to n = 1.41).

4.2.1 Geometric errors

The finite width of the liquid radiator layer implies a finite width ΔR_{geom} of the ring, as illustrated in Fig. 2. The expressions for R and ΔR_{geom} are [using Eq. (30)]

$$R = D \tan \phi = D \tan [\arcsin (n \sin \theta)] \tag{32}$$

$$\Delta R_{geom} = d \tan \theta \tag{33}$$

Note that refraction increases R but does not influence ΔR_{geom}

$$(\Delta R/R)_{geom} = (d/D)\,(\tan \theta / \tan [\arcsin (n \sin \theta)]) \,. \tag{34}$$

The effect of refraction is thus to reduce the relative geometric error in R. The reduction factor is shown as a function of n in Fig. 16. At n = 1.262 (C_5F_{12}) we have $(\Delta R/R)_{geom} = 0.65 \cdot (d/D)$. Requiring $(\Delta R/R)_{geom} < (\Delta R/R)_{chrom} = 4\%$ we obtain $d/D < 0.04/0.65 = 1/16$.

Assuming somewhat arbitrarily a N_0 value of 60 cm^{-1} one obtains for n = 1.26, using expressions (10) and (7),

$$N_{detected,max} = 60 \sin [\arccos (1/1.26)] = 22 \text{ photons/cm}$$

Assuming that of the order of 22 photons are required to determine θ (considering that some photons may be lost due to total internal reflection for inclined tracks) we could settle for d = 1 cm and would as a consequence require D > 16 cm. A lever arm of D = 20–25 cm thus seems to be a reasonable first choice.

Any further considerations with respect to geometric errors must include the fact that non-perpendicular tracks will have ellipsoidal and paraboloidal images. In a medium with n = 1.26 total internal reflection occurs for light hitting an inside surface of the medium at an angle larger than arcsin (1/n) = 52.5°. Since the maximum Cherenkov angle for n = 1.26 is θ = arccos (1/n) = 37.5°, part of the Cherenkov light is lost (leading to a paraboloidal image) when the particle trajectory is inclined by more than 15° with regard to the downstream liquid surface. This fact is illustrated in Fig. 17.

If the particle trajectory is known, an independent estimate of the Cherenkov angle can be obtained from each individual photon in an image. Since, in general, for each value of the azimuthal emission angle around the particle trajectory the chromatic and geometric errors are different the errors should be evaluated for each photon separately and then be used to calculate a weighted mean value and error for the Cherenkov angle. Figure 18, taken from the DELPHI proposed [8], illustrates for a specific case the behaviour of the geometric and chromatic errors as function of the azimuthal angle around the track.

4.2.2 Photon-positioning errors

As in the discussion on the geometric error and the requirements on the distances d and D, a precise calculation of the requirements on the spatial resolution of a photon detector

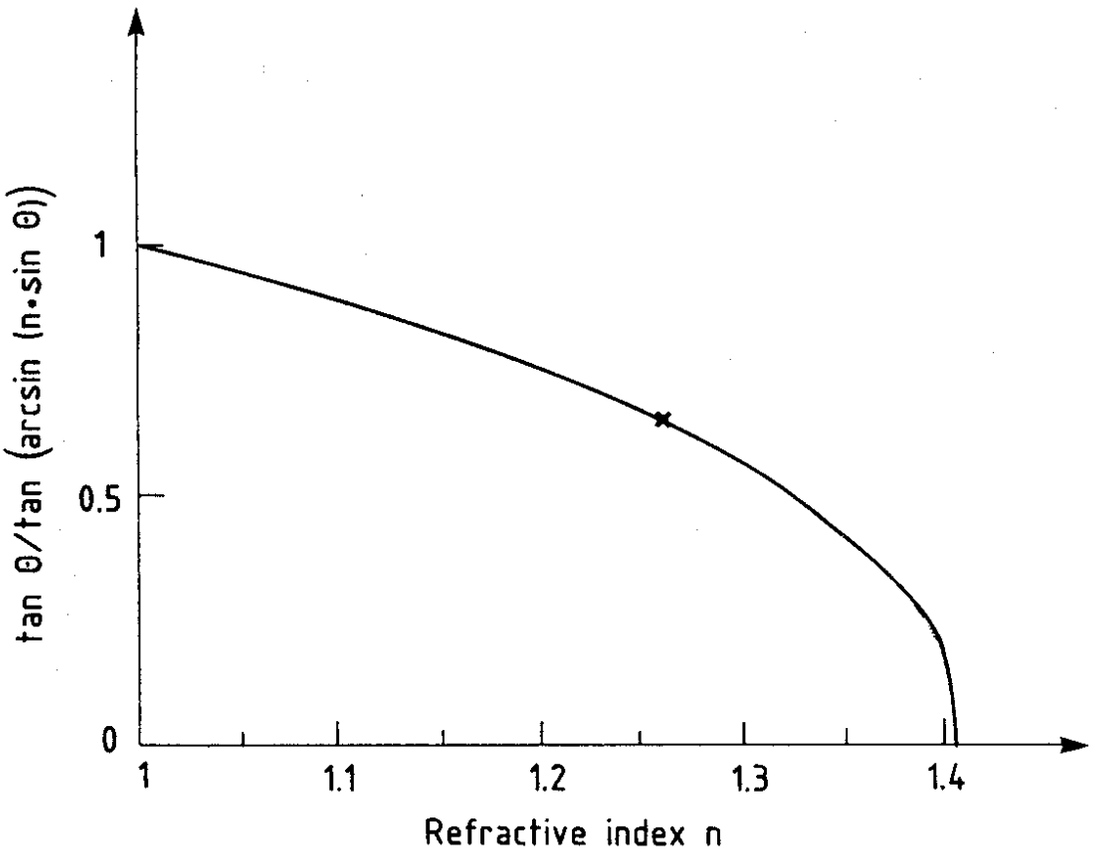

Fig. 16 The reduction factor multiplying d/D in Eq. (34) as function of refractive index n showing how the relative *geometric* resolution in Cherenkov ring radius R in a liquid-radiator RICH counter improves when going to higher values of n.

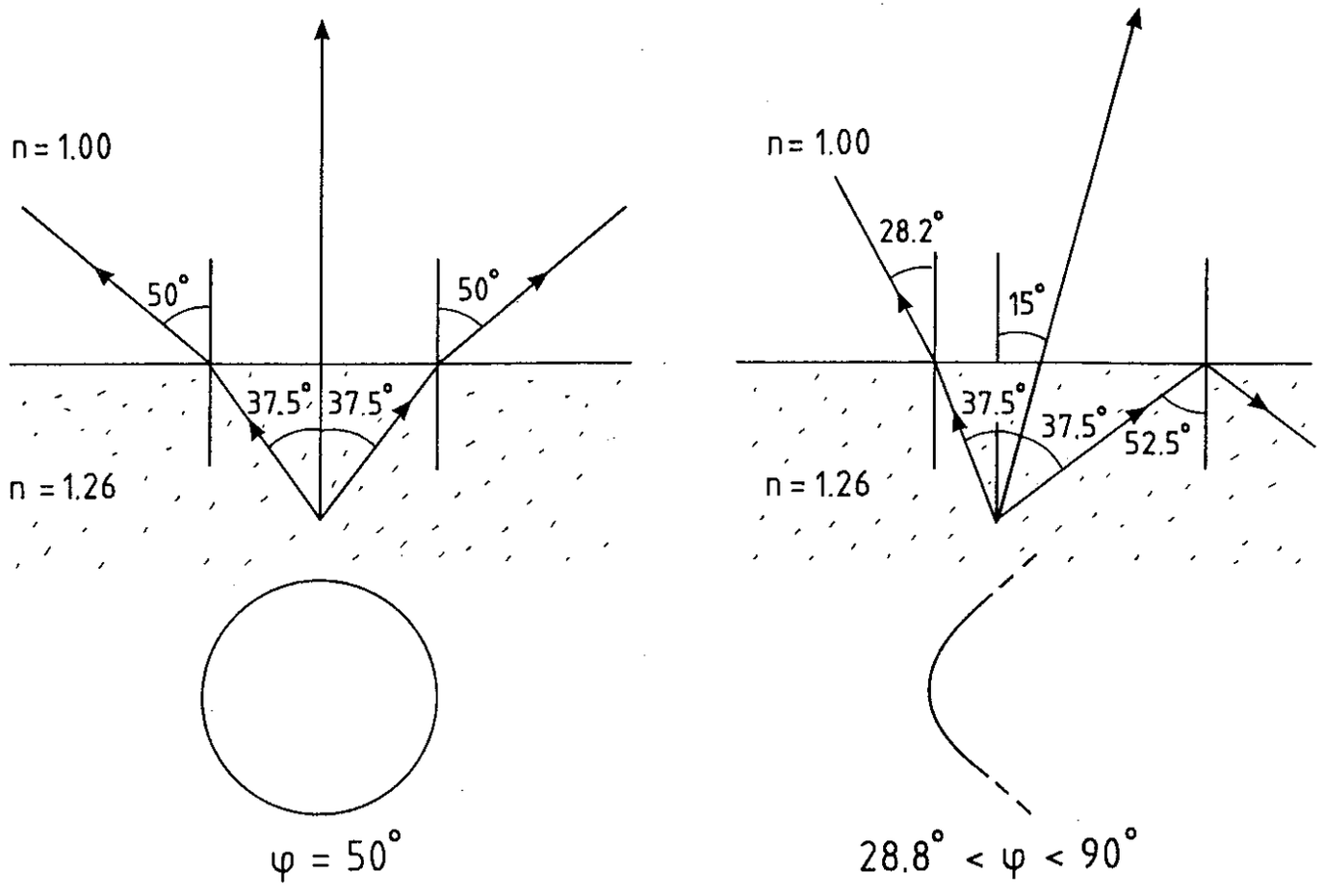

Fig. 17 The left graph illustrates how a particle of normal incidence in a liquid-radiator RICH counter produces a circular image and the right graph how a paraboloid image is obtained if the trajectory is inclined to such an extend that part of the light is totally internally reflected.

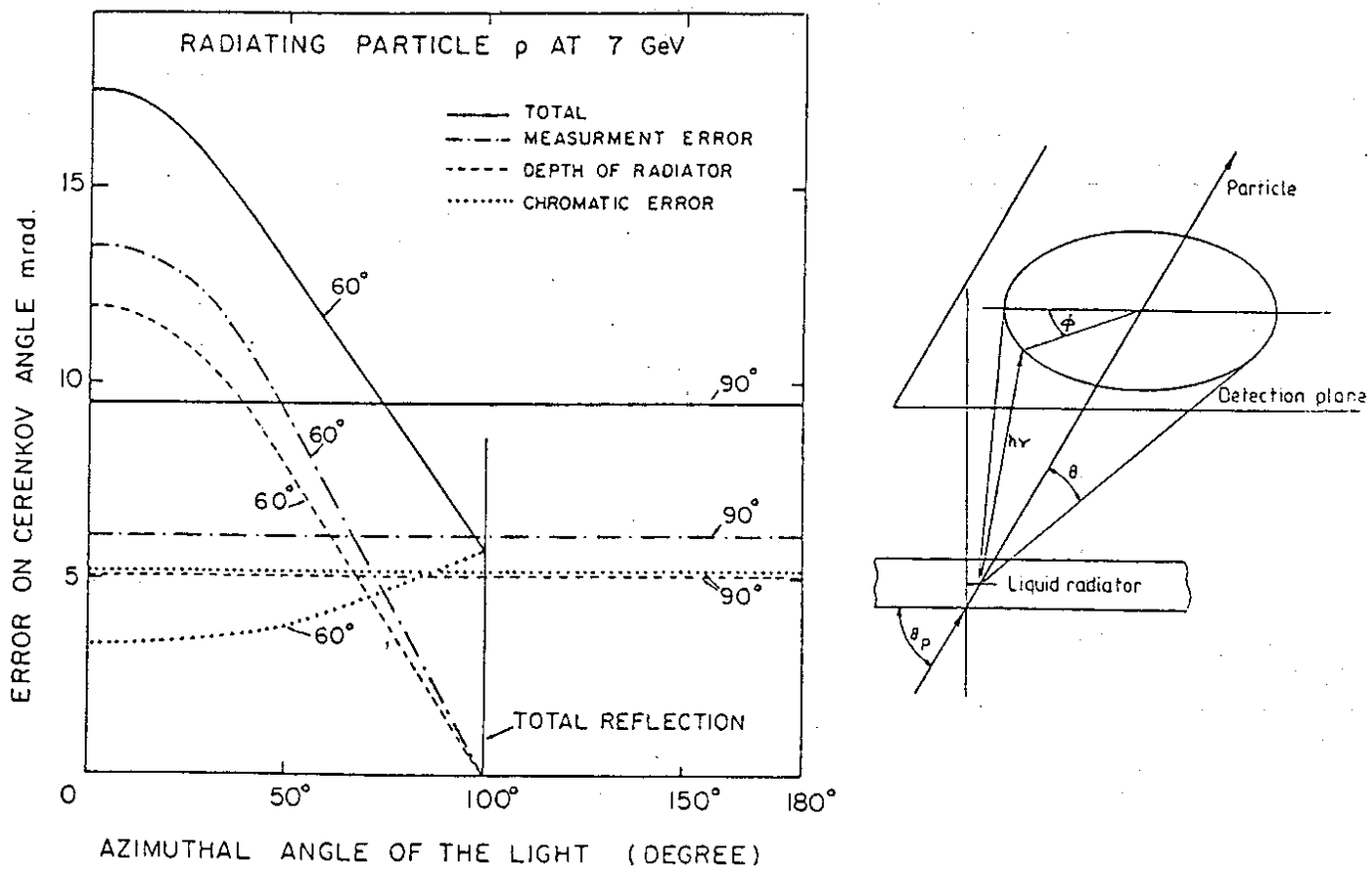

Fig. 18 Graph taken from the DELPHI technical proposal [8] showing the variation of the chromatic and geometric dispersions in the measured Cherenkov angle when the azimuthal angle around an inclined particle trajectory is varied.

cannot be made without specifying the individual case in detail. We will, therefore, limit the discussion here to some simple considerations to illustrate the first approach to the subject.

Assuming D = 20 cm and $\phi = 50°$ (n = 1.26, normal incidence) gives a ring radius of 24 cm. The requirement that $(\Delta R/R)_{xy} < (\Delta R/R)_{chrom} = 4\%$ would imply that $\Delta R_{xy} <$ 1 cm. However, inclined particle trajectories will require ΔR_{xy} to be smaller to match the higher resolution in certain azimuthal ranges around such tracks.

As to the measurement of the depth coordinate in the image plane (z) its accuracy should be of the same order as in the xy-plane since the angles we deal with are of the order of 45°.

4.2.3 Magnetic field and multiple Coulomb scattering

As already discussed, a liquid-radiator counter has a much shorter radiator and much larger Cherenkov angle as compared to a gaseous radiator counter. These two facts concur to make the relative magnetic-bend shift $(\Delta R/R)_B$ very much smaller than $(\Delta R/R)_{chrom} = 4\%$, also when taking into account that particle discrimination in a liquid radiator counter is effective at much lower momenta than in a gaseous radiator counter.

As in the case of the gaseous-radiator counter the multiple Coulomb error in R is of negligible magnitude in most practical cases.

5. SOME COMMENTS ON THE PARTICLE DISCRIMINATION POWER OF THE RICH METHOD

The purpose of the discussion in Sections 3 and 4 was primarily to relate and compare the different error-sources in the Cherenkov-angle determination in order to study their influence on the design of RICH counters. In particular, the full width $\Delta\theta$ of the spread in θ due to chromatic dispersion was compared with the full widths of the spread due to geometric errors, photon positioning errors and errors due to magnetic deflections. We will here make a few comments on how the particle discrimination power of a RICH counter is related to the parameters of the counter.

The estimator of θ in a RICH counter is in its simplest form a mean value of Cherenkov angles derived from a number $N_{detected}$ of individually measured photons. The shape of the error distribution of the one-photon Cherenkov-angle estimator is given by a convolution of the chromatic, geometric, photon position, and magnetic-bend error-functions. Once the standard deviation σ_θ of the convoluted error function is determined, the standard error in the full Cherenkov-angle estimator is obtained as $\sigma_\theta/\sqrt{N_{detected}}$, provided that there is no correlation between the measurement of the individual photons.

For example, on the simplistic assumption that the convoluted error function is Gaussian with a FWHM of $\Delta\theta$ and that there are $N_{ph} = 9$ independent determinations of θ, the standard error of their mean value is

$$\sigma_\theta = (1/\sqrt{9}) \cdot \Delta\theta/2.35 = (1/7)\,\Delta\theta\,.$$

Ideally the separation by the full spread $\Delta\theta_{chrom}$, as discussed in Sections 3 and 4, would

thus be on the very high level of seven standard deviatons if $\Delta\theta$ is interpreted as the FWHM of a Gaussian and $N_{ph} = 9$. Note that the upper velocity limits γ_{max} in Figs. 6 and 15 assume all errors other than the chromatic to be *negligible*. This will most probably not be the case in any given practical RICH counter used in a particle-collider experiment. Therefore the γ_{max} values quoted should primarily be taken as upper bounds.

In Section 3.1 the upper limit for separation of particles a and b is defined as the energy $E_{a/b}^{max}$ at which the difference $\theta_a - \theta_b$ is smaller than a certain width $\Delta\theta$, According to Eq. (19) the angular difference is inversely proportional to γ^2. This implies that a reduction of the error in θ by a certain factor will increase the upper energy-limit for particle separation only by the square-root of the same factor.

As to the lower energy limit for particle separation we have so far only referred to the absolute threshold. Since a minimal average number of photons is required for reliable detection and measurement of θ, the effective threshold is higher than the absolute threshold. If we define the normalized number of photons N_{norm} as

$$N_{norm}(\gamma_{norm}) = \frac{N_{detected}(\gamma_{norm})}{N_{detected}(\gamma_{norm} = 1)} \tag{35}$$

then relations (10) and (18) yield for small angles

$$N_{norm} = \theta^2_{norm} = 1 - 1/\gamma^2_{norm} \rightarrow \gamma^{min}_{norm} = 1/\sqrt{1 - N_{norm}} \tag{36}$$

If, for example, $N_{norm} = 1/3$ is required, then $\gamma^{min}_{norm} = 1.22$, i.e. the effective threshold is 22% higher than the absolute. The value of N_{norm} should be chosen such that the probability of having zero photons in an individual event [$= \exp(-N_{detected})$] at the effective threshold is reasonably low. (If $N_{detected} = 9$ and $N_{norm} = 1/3$, then we have $\exp(-3) = 5\%$ at the effective threshold). Note that the lower velocity limits γ_{min} in Figs. 6 and 15 represent the absolute thresholds. The γ_{min} values quoted may thus only be taken as lower bounds.

In the region between the upper and lower energy limits for acceptable particle discrimination the particle rejection factor and the particle detection efficiency are both far higher than in the regions close to these limits. Here we will not make an attempt to estimate quantitatively the levels of and relation between rejection and efficiency as a function of energy but limit ourselves to pointing out the particular features which make the RICH counter a far more discriminative detector as compared to the classical threshold Cherenkov-counter. The intrinsic granularity of a RICH counter is more than three orders of magnitude higher than that of conventional threshold Cherenkov-counter arrays (microsteradians as compared to many millisteradians) making possible the separation also of very nearby tracks. This is valuable when studying particles in jets, in particular in situations where conversion electrons cannot be avoided. The high granularity, furthermore, suppresses that particular limitation in the particle rejection of threshold counters which is due to emission of light from δ electrons.

It is finally important to remember that, as already discussed in Section 2 mass separation of particles can only be achieved through simultaneous measurement of γ and p. This implies that the momentum resolution of the magnetic spectrometer, necessary in any experiment that uses RICH counters for mass determination, may in some case be the limiting factor rather than the Cherenkov angular resolution. The upper momentum boundary most sensitive to this limitation is that for discrimination between the two heaviest particles, i.e. for K/p separation.

The above discussion does not pretend to be complete. In a real detector the error distributions have tails, measurement of individual photons are correlated, irrelevant background observations get mixed with real data, and there are systematic errors of various kinds. The effects of all this on the accuracy of θ and on the particle discrimination power can only be evaluated using a fully-fledged Monte Carlo simulation program, based on experience with prototype measurements for a given individual project. The so far quite limited experience of large-scale RICH projects in collider experiments makes it difficult to arrive at quantitative statements of general validity with regard to momentum ranges and rejection factors for particle separation. As already noted the upper and lower limits given in Figs. 6 and 15 should be taken as bounds based on reasonable but optimistic appreciation of the status and the further developement of the RICH technique.

REFERENCES

1. P.A. Cherenkov, Phys. Rev. **52**, 378 (1937).
2. See e.g. L.I. Schiff, Quantum Mechanics, McGraw-Hill, 1955, p. 267.
3. L.O. Eek, T. Ekelöf, K. Fransson, A. Hallgren, P. Kostarakis, G. Lenzen, B. Lund-Jensen, J. Séguinot, J. Tocqueville and T. Ypsilantis, IEEE Trans. on Nuclear Science **31**, 949 (1984).
4. T. Ekelöf, Possibilities and limitations of the Cherenkov ring-imaging technique at very high energies, Proc. Second ICFA Workshop in Les Diablerets, Switzerland, 1979, ed. U. Amaldi, CERN, Geneva, Switzerland, p. 396.
5. T. Ypsilantis, Phys. Scripta, **23**, 370 (1981).
6. J. Séguinot and T. Ypsilantis, Nucl. Instrum. Methods **142**, 377 (1977).
7. T. Ekelöf, Applications of the RICH technique, Proc. Int. Europhysics Conf. on High-Energy Physics, Brighton, UK, July 1983, p. 437.
8. The DELPHI Collaboration, DELPHI Technical Proposal CERN/LEPC/83-3, LEPC/P2, 17 May 1983, CERN, Geneva, Switzerland.